

A ~~semi-automatic~~ spaceborne SAR-based procedure to support the detection of ~~rapid-moving~~ landslides using spaceborne SAR imagery

Giuseppe Esposito¹, Ivan Marchesini², Alessandro Cesare Mondini², Paola Reichenbach², Mauro Rossi², Simone Sterlacchini³

5 ¹National Research Council, Research Institute for Geo-Hydrological Protection (CNR-IRPI), Rende (CS), 87036, Italy

²National Research Council, Research Institute for Geo-Hydrological Protection (CNR-IRPI), Perugia, 06128, Italy

³National Research Council, Research Institute ~~for~~ of Environmental Geology and Geoengineering (CNR-IGAG), Milano, 20126, Italy

Correspondence to: Giuseppe Esposito (giuseppe.esposito@irpi.cnr.it)

10 **Abstract.** The increasing availability of free-access satellite data represents a relevant opportunity for the analysis and assessment of natural hazards. The systematic acquisition of spaceborne imagery allows monitoring areas prone to geo-hydrological disasters, providing relevant information for risk evaluation and management. In case of major landslide events, for example, spaceborne radar data can provide an ~~innovative-effective~~ solution for the detection of slope failures, even in case of persistent cloud cover. The information about extension and location of the landslide-affected areas may support
15 decision-making processes during the emergency responses.

In this paper, we present an ~~semi-automatic~~ procedure, based on Sentinel-1 Synthetic Aperture Radar (SAR) images, aimed to facilitate the detection of ~~rapid-moving~~ landslides over wide areas. Specifically, ~~T~~he procedure evaluates changes of radar backscattered signals associated to land cover modifications, that may be also caused by mass movements. ~~The procedure~~After ~~requires an initial manual~~ a one-time calibrationsselection of some parameters, ~~and the processing chain~~ is
20 able to execute automatically the download and pre-processing of images, the detection of SAR amplitude changes, and the identification of areas potentially affected by landslides, which are then displayed in a geo-referenced map. This map should help decision-makers and emergency managers to organize field investigations. The processes automatization is implemented with specific scripts running on a GNU/Linux operating system and exploiting modules of Open Source software.

25 We tested the processing chain, in back analysis, on an area of about 3000 km² in central Papua New Guinea that in February/March 2018 was struck by a severe seismic sequence that triggered numerous widespread landslides. In the area, we simulated a periodic survey of about seven months, from 12 November 2017 to 6 June 2018, downloading 36 Sentinel-1 images and performing 17 change detection analyses automatically. The procedure resulted in statistical and graphical evidences of widespread land cover changes occurred just after the most severe seismic events. Most of them can be
30 interpreted as mass movements triggered by the main seismic shocks.

1 Introduction

Landslide recognition and mapping in rural areas represents one of the main challenges faced by the research community.

35 The spatial and temporal distribution of landslides is well known mainly in urban areas, where they often cause severe consequences to anthropic structures and population. On the contrary, landslides in rural and remote areas remain often unknown, limiting environmental evaluations like hazard and risk assessment (Guzzetti et al., 2012). Understanding where landslides have occurred may provide useful indications to forecast future events. In particular, the knowledge of the spatial distribution of landslides in a given region is essential to implement, calibrate and validate statistically and physically based
40 methods (Rossi and Reichenbach, 2016; Mergili et al., 2014a; Mergili et al., 2014b) aimed to predict the possible location of future mass movements or to identify areas where the probability of failure is negligible (Marchesini et al., 2014). As stated by Reichenbach et al. (2018), the quality and completeness of the landslide inventories may affect the reliability of the landslide susceptibility assessment (Steger et al., 2016). To produce inventory maps with limited errors and uncertainties (Santangelo et al., 2015), the mapping techniques should be selected taking into account a series of factors: the purpose of
45 the inventory, the extent of the study area (Bornaetxea et al., 2018), the scale of the base maps, resolution and characteristics of the available data, the skills and experience of the investigators, and the available resources (Guzzetti et al., 2000; van Westen et al., 2006, Casagli et al., 2017).

Besides conventional techniques (field mapping, visual interpretation of aerial photographs), remote sensing technologies based on satellite optical imagery, airborne/terrestrial laser scanning and digital photogrammetry represent innovative
50 solutions for landslide detection and mapping. ~~Recently~~In addition, ~~also~~-multispectral and Synthetic Aperture Radar (SAR) satellite images have been ~~also~~ used with great success. To recognize landslides in multispectral and Very High Resolution (VHR) optical images, the most applied methods consist in the visual interpretation (Fiorucci et al., 2011; Ma et al., 2016) or in the semi-automatic classification (segmentation) that exploits different radiometric signatures of stable and failed areas (Martha et al., 2011; Mondini et al., 2011, Alvioli et al., 2018). However, optical images have some disadvantages and
55 cannot be used when the analyzed areas are covered by persistent clouds or affected by shadow effects. To overcome these issues, SAR data can represent an effective alternative, since they are not ~~much~~ influenced by weather conditions.

Several techniques allow extracting information from SAR data to identify and map slope failures. The Differential Interferometric Synthetic Aperture Radar (DInSAR) (Gabriel et al., 1989) has been widely used to detect surface displacements over large areas with sub-centimeter accuracy. DInSAR is aimed to calculate phase differences between two
60 or more multi-temporal images and has been successfully applied to analyze landslides (Calò et al., 2012; Zhao et al., 2012; Cigna et al., 2013; Calvello et al., 2017; Tessari et al., 2017), earthquakes, subsidence, soil consolidation, volcanoes and tectonic deformations (Plank, 2014 and references therein). Other techniques exploit the amplitude information contained in the pixels of the SAR images. Amplitude of the backscattered signal is influenced by the type of target and varies according to several factors, such as the type of land use (e.g., water bodies, ice cover, forest type, bare soil), the surface roughness and
65 the terrain slope. According to Colesanti and Wasowski (2006), amplitude SAR imagery represents potentially a very useful

source of information, which can complement high resolution optical imagery and aerial photography in feature detection. Generally, amplitude-based methods analyze the correlation of the speckle pattern of two images (e.g., pre- and post-event, where the terms “event” can refer to a major natural and/or human-induced hazard affecting a given area, as an earthquake, a hurricane, a forest fire, etc.) to map the land cover changes (Raspini et al., 2017). To date, the landslide mapping community has shown a poor attitude in using this type of product, so that only few studies have demonstrated the valuable contribution of SAR amplitude changes in landslide detection and mapping. According to Mondini (2017), this is due to a series of problems and drawbacks represented by: 1) the complex pre-processing procedures; 2) [geometric distortions, the such as layover and shadowing due to the side-looking acquisition geometry of SAR sensors](#), that can affect the quality of the images over mountainous areas, where landslides are likely to occur; 3) the difficulty in using the SAR signal in traditional statistical classification approaches mainly due to speckling. A successful example of the use of amplitude variations of the radar signal to analyze landslides is described by Zhao et al. (2013), which inferred the Jiweishan rock slide in China using changes in SAR backscattering intensity in ALOS/PALSAR images. Tessari et al. (2017) verified that when the phase information cannot be exploited, amplitude of the reflected signal is very useful to detect and map rapid-moving landslides that cause significant variations in the ground morphology and land cover. Mondini (2017) proved that both landslides and flooded areas can be detected by verifying changes in the spatial autocorrelation in a multi-temporal series of SAR images. Konishi and Suga (2018) also identified a series of landslides in Japan by analyzing intensity correlation between pre- and post-event SAR images.

Besides the described techniques, recent advances in SAR technology are promoting the use of polarimetric SAR data (PolSAR) characterized by full-polarimetric information (i.e., acquired in single polarization, dual polarization, and fully polarimetric modes) for a target in the form of the scattering matrix (Skriver, 2012). According to Plank et al. (2016), these data provide more information on the ground, which enables a better land cover classification and landslide mapping. Successful applications were described by Yamaguchi (2012), Shimada et al. (2014), Li et al. (2014) and Plank et al. (2016). The use of SAR data to analyze landslides and/or potentially unstable slopes should hence increase, also in relation to a series of valuable technical innovations. The improved revisiting times and spatial resolution of the images, for example, represent a key factor during disaster response operations, when a preliminary localization of areas potentially affected by major landslides is crucial. Revisiting times have been in fact reduced from 35 days of ERS and Envisat satellites, to 12 hours (at 40°latitude, in case of emergency response) of the COSMO-SkyMed constellation (Casagli et al., 2017). The enhanced spatial resolution ([azimuth or along-track resolution](#) x range [or across-track resolution](#)) of images spans in the order of few meters (i.e. 1-10 m), resulting more detailed with respect to the [coarser](#) resolution of the first-generation satellites characterized by pixel sizes ~~of 10-30~~ [up to 100](#) meters (Plank, 2014).

Among the most advanced SAR spaceborne systems (Casagli et al., 2017), there are those of the mission Sentinel-1 operated by the European Space Agency (ESA) in the frame of the European Union’s Copernicus Programme. Satellites Sentinel-1A and 1B acquire images characterized by ~~a spatial resolution~~ [pixels with sizes ranging from 5 \(range\) × 20 \(azimuth\) m, in the default acquisition mode for land observations \(Interferometric Wide Swath mode - IW\)](#), up to 5x5 m, ~~depending on the~~ in

100 the Strip Map acquisition mode, ~~and a~~ The temporal resolution ranges ~~ing~~ from 6 to 12 days according to the surveyed geographic area. The Sentinel-related products have a global coverage and are freely available to all users registered on the ESA data hub (<https://scihub.copernicus.eu/>). This is a considerable benefit that is leading many research institutions and public administrations to use Sentinel data to investigate landslides and other natural processes (Salvi et al., 2012; Dai et al., 2016; Twele et al., 2016; Intrieri et al., 2018). According to Raspini et al. (2017), the future increased number of available
105 satellites characterized by shorter revisiting times and high spatial resolution will offer relevant information for decision support and early warning systems. Currently, significant limitations concern the real-time and/or quasi real-time detection of rapid flow-like mass movements, rock failures, and flash floods characterized by evolution times ranging from minutes to hours. This poses a challenge for the geo-hydrological risk management based on satellite technologies.

In this article, we present an ~~semi~~-automatic procedure aimed to support the detection of rapid-moving landslides by
110 performing the periodic survey of unstable slopes, using spaceborne radar imagery. We focus on rapid-moving landslides since they determine evident land cover changes with respect to slow-moving failures. The main purpose of the implemented procedure is to emphasize areas where ~~evident~~ land cover changes (potentially related to slope failures) ~~have occurred~~, facilitating the following possible phases of mapping and/or field surveys. In other words, the procedure allows producing a map ~~where pixels are ranked based on the level of~~ that highlights the land cover changes observed by comparing two
115 consecutive ~~satellite~~-spaceborne SAR images. Decision makers and emergency managers can use this map to organize possible verifications and field investigations.

The procedure is implemented in a processing chain based on free data and software, and exploits radar backscattered signals recorded within the Sentinel-1 SAR images. The values of some parameters related to the used algorithms must be provided by the user. In alternative, they can be set based on the values derived from other similar areas. The processing chain was
120 applied, in back analysis, to an area in Papua New Guinea that in February/March 2018 was struck by a severe seismic sequence, which triggered numerous widespread landslides.

2 Methodology

2.1 Pre-processing of SAR images

The implemented procedure is based on Sentinel-1 images available in Level-1 Single Look Complex (SLC) ~~mode~~, with a
125 VV-VH polarization and Interferometric Wide acquisition mode. Level-1 SLC products are images provided in slant range geometry, georeferenced using orbit and attitude data from the satellite. Each image pixel is represented by a complex magnitude value and contains both amplitude and phase information (ESA, 2018). Pre-processing of the images is performed

using the Graph Processing Tool (GPT) of the Sentinel-1 Toolbox¹, and includes the following steps: (1) thermal noise removal, (2) radiometric calibration, (3) Topsar de-burst, and (4) multi-looking processes.

130 The thermal denoising consists in the removal of dark strips with invalid data from the original data. This operation is performed with the SNAP algorithms by subtracting the noise vectors provided by the product annotations from the power detected image (ESA, 2017); the radiometric calibration allows ~~computing the slant range radar brightness coefficient (β_0) (El-Darymli et al., 2014) by~~ converting digital pixel values in a radiometric calibrated backscatter (β_0) (El-Darymli et al., 2014); the Topsar de-burst removes black-fill demarcations between the single bursts forming sub-swaths of the IW-SLC products, allowing retrieving single images; ~~and the~~ multi-looking process is carried out to reduce the standard deviation of the noise level and to obtain approximately square pixels of about 14 m (mean ground resolution), by applying a factor of 1:4 (azimuth:range).

Consecutive SAR images, selected to detect amplitude changes of the radar signal (i.e. change detection), are co-registered with a DEM-assisted procedure that uses the Shuttle Radar Topography Mission (SRTM) 1 Sec digital elevation model (DEM), auto-downloaded by SNAP. After the co-registration, the resulting stacked images are filtered for speckling reduction using the adaptive Frost filter (Frost et al., 1982), with a filter size in X and Y of 5 pixels, and a damping factor (defining the extent of smoothing) of 2.

2.2 Detection of SAR amplitude changes

To perform the change detection analysis, the Log-Ratio (LR) index is calculated as described by Mondini (2017). This index measures the change in the backscattering that might be induced by land cover changes related to both natural (e.g., landslides, floods, snow melting) or human-induced processes (e.g., mining activities, deforestation), in a defined time interval. For each pair of corresponding pixels belonging to consecutive pre-processed SAR images, the Log-Ratio index is calculated as follows:

$$150 \quad LR = \ln \left(\frac{\beta_{0,i}}{\beta_{0,i-1}} \right) \quad (1)$$

where ~~β_0 is the radiometric calibrated backscatter (i.e., SAR amplitude), and $\beta_{0,i}$ and $\beta_{0,i-1}$ i-1~~ indicate two consecutive backscatter values two consecutive pre-processed SAR images. For each pair of pre-processed images, a LR layer is computed, and related pixels can be characterized by positive or negative values, depending on the backscattering changes.

When the study area (i.e. Area of Interest - AoI) corresponds to a zone smaller than the entire LR layer, a subset is extracted by using the subset tool in SNAP.

¹ GPT is the Command Line Interface of the Open Source software SNAP Sentinel Application Platform, version 6.0 - <http://step.esa.int/main/toolboxes/snap/>. The source code of SNAP is available at <https://github.com/senbox-org>

2.3 Segmentation of the Log-Ratio layer

The segmentation of the LR layer is aimed to group pixels with similar LR pixel values into unique segments. The process is performed with the i.segment module in GRASS GIS 7.4 (Momsen and Metz, 2017), using the “Mean Shift” algorithm and the adaptive bandwidth option.

160 The first step of the Mean Shift algorithm consists in the smoothing process of the LR layer. To do this, the algorithm requires from the user the definition of the following parameters: (i) the initial bandwidth size (hr); (ii) the spatial kernel size (hs); (iii) the threshold (th), and (iv) the maximum number of iterations. We acknowledge that the smoothing considers the pixel p (having value LR_p) in the center of a spatial kernel of size hs and assigns to this a mean value calculated using only the pixels that are inside the spatial kernel and, with values ranging between $(LR_p - hr)$ and $(LR_p + hr)$. The unit of measurement of hs is in pixel and hr is a range of LR values. In other words, the smoothing allows that each pixel value is computed considering all pixels not farther than the spatial kernel (hs) with a difference not larger than hr . This means that pixels that are too different from the considered pixel p are not included in the calculation of the new value.

165 With the adaptive option, for each pixel p , hs is fixed whereas the bandwidth size $(hr_{ad})_p$ is recalculated to account for the variation of the pixels values (LR in this work) across the spatial kernel centered in p . The aim is to avoid the drawbacks of a global bandwidth consisting in under- or over-segmentation. More in general, the adaptive bandwidth size (hr_{ad}) is calculated using the following equation:

$$(hr_{ad}) = avgdiff \cdot \exp\left(-\frac{avgdiff^2}{2 \cdot hr^2}\right) \quad (2)$$

175 where $avgdiff$ is the average of the differences between the value of the central pixel and the values of other pixels included in the kernel; hr_{ad} is maximum if the $avgdiff$ is equal to the user-defined hr , which is also the upper limit of the possible hr_{ad} values (i.e. hr_{ad} is always smaller than hr). The adaptive option is particularly useful when data are characterized by high and abrupt spatial variability (as is the case of the LR layers), and a smoothing preserving the main discontinuities is required (Comaniciu and Meer, 2002).

180 The Mean Shift algorithm recalculates the central pixel values until a user-defined maximum number of iterations is reached, or until the largest shift (value difference) resulting between the central pixel and the pixels inside the kernel is smaller than a threshold (th) defined by the user. The threshold must be bigger than 0.0 and smaller than 1.0: a threshold of 0 would allow only pixels with identical values to be considered similar and clustered together in a segment, while a threshold of 1 would allow everything to be merged in a very large segment (Momsen and Metz, 2017). A more or less conservative threshold
185 needs to be chosen considering the spectral properties of the analyzed image. After the smoothing, pixels in the range of the estimated local maxima (Comaniciu and Meer, 2002), which are close to each other, are clustered and included in a new

raster map containing the defined segments. To reduce the “salt and pepper effect”, the segments containing less than a preferred minimum number of pixels are eliminated, by specifying the *minsize* parameter within the *i.segment* command.

To select the appropriate parameter values (i.e. tuning), a specific analysis should be carried out interactively (manually) before the implemented procedure is started. In particular, variability of the segmentation outcomes to the usage of different values for the *hs*, *hr* and *th* parameters must be analyzed. This analysis is event-dependent because it can be executed using consecutive SAR images acquired before and after a well-known landslides event occurred in the past, in the area to be surveyed or in areas which are considered similar by geomorphologists, based on the types of land cover and expected types of landslide. The spatial kernel size *hs* can be heuristically chosen according to the size of the land cover changes that should be detected. Keeping constant the spatial kernel size, *hr* and *th* values can be changed iteratively, evaluating the results in terms of number and sizes of segments generated by the Mean Shift algorithm. As general rule, one can expect that large values of *hr* will correspond to few (but big) segments, whereas small values of *hr* will determine many small segments. This is due to the fact that smoothing increases when larger values of *hr* are used. The effect of the variation of the value of *th* is expected to work in the opposite direction but being much less effective on the segmentation outcomes. The first scenario (few and very large segments) is useless since it cannot be used for geo-localize the possible land cover changes. The second scenario (many and small segments) is the result of the segmentation of the random noise of the back-scattered SAR images and it is, again, useless. We assume that a possible criterion for selecting the best values of *th* and *hr* is to search for the combination of values that optimize, at the same time, the number of segments and their average size with respect to the expected land cover changes. An example of the procedure for the selection of the best values for the *th* and *hr* parameters is described in section 3.

2.4 Identification of areas potentially affected by land cover changes

After the segmentation step, a statistical analysis of the LR values included in each segment is carried out to identify segments that, with high probability, are related to significant land cover changes.

For each segment, the arithmetic mean (μ_s) of the included LR pixel values is calculated as follow:

210

$$\mu_s = \frac{1}{k} \left(\sum_{j=1}^k p_j \right) \quad (3)$$

where *s* indicates the segment, *p* the pixel value and *k* the number of pixels in the segment. We define as “average layer”, the raster layer where at each segment is associated the corresponding value of μ_s . Afterwards, in order to filter segments and extracting only those representing significant statistical changes, the μ_s values have to be compared with reference μ and average standard deviation ($\bar{\sigma}$) related to no-change conditions. These reference figures have to be calculated before the

215

initialization of the processing chain and after the segmentation of the event-related LR image, using preceding SAR images when no heavy rainfall, landslides and earthquakes occurred, by applying the following formulas:

$$\mu = \frac{1}{m} \left(\sum_{j=1}^m p_j \right) \quad (4)$$

220

$$\sigma_s = \sqrt{\left(\frac{1}{k-1} \right) \left(\sum_{j=1}^k p_j - \mu_s \right)^2} \quad (5)$$

225

$$\bar{\sigma} = \frac{1}{r} \left(\sum_{z=1}^r \sigma_{s_z} \right) \quad (6)$$

where m is the total number of pixels in the pre-event LR image used as reference, p is the related pixel value, and r is the total number of segments derived from the segmentation of the event-related LR image, characterized each one by a σ_s .

230 In this way, both the μ and $\bar{\sigma}$ are calculated in a kind of “warm-up stage” of the described processing chain. Generally, ~~suitable~~ these reference figures can be ~~considered as suitable if~~ calculated ~~since the generation of~~ from three or four reference LR layers characterized by values normally distributed (i.e. Gaussian); ~~Such distribution in fact indicates~~ing a random nature of the LR ~~values, distribution~~ that is typical ~~of no significant~~ when land cover changes ~~are not relevant~~. We highlight that, in such a case, given that LR values are ~~typically commonly~~ small and positive or negative, the μ value is equal or very
235 close to zero.

In this way, all the segments of the “average layer” characterized by μ_s values larger than $|\mu+(2\bar{\sigma})|$ are then extracted and classified. Segments with μ_s values lower than a confidence interval of 95% ($\mu_s < |\mu+(2\bar{\sigma})|$) are instead discarded. Segments where μ_s is greater than $|\mu+(2\bar{\sigma})|$ and smaller than $|\mu+(3\bar{\sigma})|$ are reclassified to the integer value of 2. Similarly, the values 3 and 4 are used to classify segments with μ_s values included in the range $|\mu+(3\bar{\sigma})|$ to $|\mu+(4\bar{\sigma})|$, and larger than $|\mu+(4\bar{\sigma})|$,
240 respectively. All these segments form a new raster layer representing a map of areas characterized by relevant SAR amplitude changes, including those affected by rapid slope movements.

In order to refine this map, all the segments with the same values (i.e., 2, 3, or 4), that are spatially contiguous and are formed by at least a user-defined minimum arbitrary size in terms of pixels (i.e. minimum detectable landslide area) are merged together, and the following statistics are then computed: 1) count of merged segments; 2) maximum number of
245 pixels included within a single segment; and 3) average number of pixels included within a single segment.

The final segment map produced by the ~~semi-automatic-processing~~ chain is georeferenced in the WGS84 reference system (EPSG 4326) by means of the Terrain correction tool of SNAP.

2.5 ~~Script~~ Automatic implementation of the processing chain

250 The processes described before have been implemented in two groups of scripts that can be executed automatically (in-chain), according to the flowchart shown in Figure 1. They are run after a preliminary one-time calibration phase, operated manually by the user and consisting of: 1) the tuning of the `i.segment` parameters, carried out with the expert-based segmentation of an event-related LR image (paragraph 2.3); 2) the computation of reference μ and $\bar{\sigma}$ related to no-change conditions, as described in the paragraph 2.4.

255 ~~Besides segmentation of the event related LR image with tuning of related parameters, and the calculation of reference μ and $\bar{\sigma}$ related to no-change conditions, all the other described procedures have been implemented in two groups of scripts that can be executed automatically.~~

260 The python-based script (Fig. 1, Data ingestion) is devoted to the automatic querying and downloading of Sentinel-1 SAR images from the ESA Sentinel Data Hub. The script, based on the SentinelSat toolbox (Kersten et al., 2018), is set to query the Sentinel Data Hub with a daily frequency, even though new images may be available every 6 or 12 days, depending on the geographic area.

265 The `consecutive` group of scripts, written in GNU/Bash programming language (Fig. 1), is aimed at: (i) pre-processing the Sentinel-1 images (section 2.1), (ii) detection of the changes in SAR amplitude and production of Log-Ratio maps (section 2.2), (iii) segmentation of the LR maps (section 2.3) and, (iv) identification of areas potentially affected by land cover changes (section 2.4). This group of scripts is executed automatically when new Sentinel-1 images are available and downloaded by the python-based script.

270 The bash-scripts require the following settings defined by the user: 1) the path of the folder where the downloaded SAR images are stored; 2) values of the parameters ~~required to use~~ for the segmentation (see section 2.3), and (3) the spatial coordinates of the area of interest (if it is a portion of the downloaded SAR images). No further information is needed since the commands are executed in a unique automatic sequence. To survey the same area for an unlimited time period, all these settings have to be defined only `one time` for the chain initialization.

3 The Papua New Guinea test site

275 We selected as test site, an area located in central Papua New Guinea (Fig. 2) that was affected by a severe seismic sequence at the beginning of 2018. On 25 February, the area was hit by a main seismic event (M7.5) followed by several aftershocks, including a M6.7 earthquake on 6 March. The strong mainshock, rather superficial with a hypocentral depth at 23.4 km (USGS, 2018), caused building collapses, road damage and widespread landslides mostly along the Tagari river valley and

the slopes of Mount Sisa (McCue et al., 2018). According to the International Federation of Red Cross and Red Crescent Societies (IFRC, 2018), more than 100 people died, most of them due to landslides.

To test the implemented procedure, we ~~have~~ analyzed an area of about 3000 km² in the mountainous region close to the epicenters of the mainshock (Aoi in Fig. 2), where preliminary information on landslides were available (Petley, 2018a, b).

280 To simulate a periodic survey covering pre- and post-earthquake periods, we downloaded 36 Sentinel-1 images from the Sentinel Data Hub (<https://scihub.copernicus.eu/>) acquired along the satellite track n.82 ~~in ascending orbit~~ with a temporal frequency of 12 days, from 12 November 2017 to 6 June 2018. ~~Considering that the majority of the slopes in the study area are exposed towards West, to limit geometrical distortions in the single images and in the change detection estimation, we preferred to use IW-SLC products acquired in ascending mode, with a VV-VH polarization. Each IW product is collected~~
285 ~~with a swath characterized by a width of 250 km, subdivided in turn to three sub-swaths containing one image per polarization, consisting of a series of bursts which are processed as independent SLC images.~~

The downloaded images were used to perform a total of 17 change detection analyses which resulted in likewise LR layers, with a pixel size of about 14 m. The values of the segmentation parameters were defined with an interactive manual analysis (see section 2.3) by segmenting the “pre-post M7.5 earthquake” LR layer, selecting the spatial kernel size (*hs*) of 10 pixels
290 (see section 2.3), and setting the maximum number of iterations to 200. This size of the spatial kernel was set to 10 pixels to detect significant differences of LR values during the smoothing stage of the segmentation process, taking into account the approximate expected size of the land cover changes. In the interactive (manual) analysis, we selected bandwidth sizes (*hr*, see section 2.3) ranging from 0.0005 to 0.016, and thresholds (*th*) from 0.001 to 0.016 (Fig. 3), obtaining 20 different parameter combinations. For each couple of parameters, the number of generated segments and their average size were
295 ~~as shown~~ in Fig-ure 3. Points highlight the major impact of the *hr* parameter with respect to the role played by the threshold (*th*) parameter, in defining the number of total generated segments. Below an *hr* value of 0.004 over segmentation occur, whereas for *hr* values equal or larger than 0.004, the number of generated segments tends to become small and constant. With the aim of avoiding over segmentation while maintaining a reasonable average size of the segments (to be able to delineate also small patches of the terrain where changes occurred), and considering a visual inspection of the
300 segmentation results ~~obtained with the different combinations~~, we decided to run i.segment in the ~~semi~~-automatic processing chain using the following set of parameters values: *hs*=10, *hr*=0.004, *th*=0.008, *minsize*=2, *iterations*=200 (see section 2.3).

After the segmentation of the 17 LR layers, ~~areas affected by layover and shadowing effects were masked out in order to avoid errors in the statistical analysis described below and in the localization of potential landslides. The mask was developed in SNAP by means of the SAR Simulation Terrain Correction tool, exploiting the SRTM 1Sec DEM.~~

305 ~~†~~The segments with a minimum size of 5 pixels were extracted in the area of interest (an example ~~is shown~~ in Fig. 4d), and statistics were calculated according to the confidence intervals described in the methodology section. We decided to select only the segments with a minimum size of 5 pixels, corresponding to a minimum area of about 980 m² (i.e. a single-pixel area roughly equal to 196 m² ~~times~~ 5 pixels), after a ~~rough~~-general evaluation of the preliminary landslide-related images published on news websites and social networks, and considering that the ~~occurrence~~-detection of smaller ~~mass~~

310 ~~movements~~segments in the test area ~~were~~was not significant at the scale of our analysis for detecting landslides. It is worth noting that accuracy of such a minimum area is not accurate due to the use of a geographic (not projected) reference system (WGS84).

In Fig-~~ure~~ 5, statistics of the selected segments are displayed for each change detection. The analysis of the histograms revealed ~~that~~two main peaks ~~occurred for~~corresponding to the change detections 9 and 10. Change detection 9 considers
315 images acquired before and after the M7.5 earthquake, whereas change detection 10 the images acquired on 28 February and 12 March 2018. The first peak highlights widespread changes related also to landslides extensively documented after the M7.5 event (Petley, 2018a). The second peak was instead unexpected and was probably due to the occurrence of further landslides triggered by the M6.7 event on 6 March 2018. In Fig-~~ure~~ 6, segments related to these two peaks are displayed (red pixels = change detection 9; blue pixels = change detection 10). To check whether these segments were effectively located in
320 areas characterized by a high concentration of seismic-induced landslides, we analyzed optical images available on the Planet explorer application (Planet, 2017). By means of a visual interpretation, we identified the zones (the yellow polygons shown in Fig. 6) where clusters of landslides occurred, verifying a general accordance with the spatial distribution of both red and blue segments. ~~The map shows that the two groups of segments are in general accordance with the areas (in yellow) really affected by landslides, as interpreted from the optical images available on the Planet explorer application (Planet, 2017).~~
325

Small widespread segments outside the ~~landslide~~areas affected by landslides, mostly related to stream changes and noise, also resulted in the AoI. Similar random segments occurred in the pre- and post-event change detections, as also displayed by statistics in Fig-~~ure~~ 5.

3.1 Statistical evidence of landslide-like segments

330 ~~Clear e~~Evidence of the widespread land cover changes induced by the two earthquakes, as well as the timing of their occurrence, resulted also from a statistical analysis of the segment areas derived from each change detection. The comparison of some representative statistics of segment's areas related to different change detections are shown in Fig-~~ure~~ 7. For each comparison, four types of statistics are displayed: Quantile-Quantile (Q-Q) plot, Empirical Cumulative Distribution Function (ECDF), Density plot, Frequency plot.

335 The first column in ~~Figure~~. 7 compares areas of the segments resulted from the change detections 11 and 7, which we assume not being affected by landslides triggered by the earthquake (i.e., NO-EVENT/NO-EVENT, where the term EVENT refers to the earthquake shocks); the second column shows the comparison between areas of the segments resulted from change detections 6 and 10, with the second including seismic-triggered landslides (i.e., NO-EVENT/EVENT); the third column indicates the comparison between areas of the segments from the change detections 9 and 10, both with landslides
340 (i.e., EVENT/EVENT).

Clear differences can be noted between the areas distribution of segments with and without landslides (change detection 6 - change detection 10) displayed in the NO-EVENT/EVENT plots. This difference is particularly highlighted in the Q-Q plot,

where the gap between the blue line representing the real distributions and the theoretical similarity condition (red line) is evident.

345 ~~Taking into account~~Considering the p-values from the Kolmogorov-Smirnov tests carried out for all the 136 distribution comparisons (the combination of 17 change detections taken 2 at a time without repetition), it arises a general similarity (i.e. p-value > 0.05) among ~~86-81~~ of the ~~95-105~~ distributions that were not affected by landslides (NO-EVENT/NO-EVENT) (Fig. 8). On the other hand, among the 30 NO-EVENT/EVENT distributions, the majority (21/30) are different. The EVENT/EVENT distribution is ~~also different~~instead the same (Fig. 8).

350 We have attempted to analyze the distribution of the areas of the segments derived from the change detections to verify if they followed the empirical statistical distribution of the landslides size, as described by different theoretical models (Stark and Hovius, 2001; Malamud et al., 2004; Rossi et al., 2012; Schlögel et al., 2015).

By using the tool implemented by Rossi et al. (2012) for estimating the probability distribution of landslide areas, we verified that medium and large-scale areas of segments obtained with the change detections 9 and 10 followed a landslides-like behavior. In fact, the two probability distributions obtained with a Double Pareto Simplified model (Fig. 9) resulted in inverse power law decays for medium and large areas, highlighting a moderate agreement with empirical data. A rollover (inflection) in correspondence of small areas (e.g., Malamud et al., 2004) however is not present. This can be due to a consistent detection of small changes (i.e. $\sim 1000 \text{ m}^2$) ascribable to landslides and other random land cover modifications, other than some noise. In addition, it is worth remembering that segments with areas $\leq 980 \text{ m}^2$ were not considered.

360 As shown in Fig-ure 9, the two analyses did not pass the Kolmogorov-Smirnov test (p-value = 0). This may be explained with the fact that the input datasets (i.e. segments area) were not obtained with a proper landslide mapping activity, as described in Guzzetti et al. (2012), but with a ~~semi-automatic~~ procedure that is not aimed at landslide mapping operations, as clarified in the Introduction section, but at identifying land cover changes also related to landslides. Although this, results seem to be fair consistent with curves of proper landslide inventory data (Schlögel et al., 2015).

365 4 Discussion

In this article, we describe a ~~semi-automatic~~ processing chain aimed at identifying SAR amplitude changes that can be partially explained by the occurrence of ~~rapid~~ mass movements. We have selected SAR data since they have the advantage to be not affected by the cloud cover disturbance. In fact, as described by Mondini et al. (2019), the use of SAR amplitude data can mitigate the cloud coverage issue and can allow detecting landslides that, otherwise, might remain unknown or
370 unnoticed for a long time. In this way, the procedure can be exploited for a “continuous”, in terms of time, slope monitoring activity, even if failures occur during long-lasting periods of precipitation and persistent cloud cover that do not allow to use optical data for a rapid and detailed landslide recognition. In the selected study area, a widespread cloud cover persisted for several weeks during and after the seismic sequence. The first cloudless optical image of the area damaged by the seismic shaking was published by the daily monitoring service delivered by ©2019 Planet Labs Inc. (www.planet.com) on 25 March,

375 almost one month after the M7.5 mainshock that triggered numerous landslides. The high cloud persistence is quite common in Papua New Guinea, and in fact this is included in the cloudiest regions of the world with annual cloud frequency (proportion of days with a positive cloud flag) higher than eighty percent (Wilson and Jets, 2016; Mondini et al., 2019). As consequence, the use of optical data in this area, and in other mountainous regions exposed to prolonged rainfall related to monsoons, cyclones or other persistent meteorological systems results tricky.

380 The obtained results depend on the definition of the image pre-processing and segmentation parameters that should be calibrated a priori (see sections 2.3 and 2.4). While images geometric and radiometric corrections are quite standard and well-accepted procedures, the SAR multiplicative noise filtering remains a largely discussed point in the scientific literature and there is not a consensus on the selection of strategies. We choose the Frost filter because it already proved to be properly working in mountainous environments (Schellenberg et al., 2012) and it was used successfully in previous studies dealing
385 with landslides (Mondini, 2017). We acknowledge that different filters might have brought different results or requested a different tuning of the segmentation procedure. The impact of different filters on our procedure might be an interesting follow up of this work. Another improvement may consist in the use of images acquired in both ascending and descending geometries. The use of ascending images was only related to focus this first step of the work on the implementation of the entire processing chain, that we tried to simplify as much as possible. In fact, there is no doubt that combining images
390 acquired in ascending and descending geometries can improve the quality of results, representing a non-trivial advancement of the procedure that was out of the aim of this first implementation. The a priori choice of using ascending products was based on the findings that most of the slopes in the study area are exposed towards West, with the aim of limiting the inclusion of geometrical distortions in the change detection products.

The tuning of the segmentation parameters is the key element for identifying areas affected by significant land cover changes, also induced by rapid-moving slope movements. This process can be retained event-dependent, requiring a well-
395 known landslide event occurred in the past in the analyzed area or in zones with similar topographic and land use characteristics. In the case study here described, definite values of the segmentation parameters were obtained by segmenting the pre-post M7.5 earthquake LR layer, and by testing different values combinations (Fig. 3). This may represent a limit of the proposed procedure if one would apply it in different geomorphic settings without past landslide events, or identifying
400 different types of slope failures. On the other hand, if a proper event-based tuning operation is performed, a continuous monitoring of slopes can be efficiently ~~carry~~-carried out without temporal limitations, exploiting both pre- and post-event available images, as done in the current case history. The described application highlighted in fact that by keeping the same parameters values, ~~landslides and other~~ land cover changes triggered by the M6.7 aftershock were also detected. **Overlapping**
405 **between the calculated segments (i.e. change detections 9 and 10) to ground truth data revealed that largest SAR amplitude changes corresponded often with landslides (Fig. 6). A further evidence was provided by the statistical distributions shown in Figure 9, resulted similar to those estimated by other landslide-related studies (Stark and Hovius, 2001; Malamud et al., 2004; Rossi et al., 2012; Schlögel et al., 2015). The segments located mostly outside the areas affected by landslides were caused instead by other land cover changes that were out of the aims of this study, or by random noise effects. Segments**

related to these changes can be easily identified because composed by an average number of pixels close to ten, as detected
410 in all the change detections, whereas segments related to landslides (i.e. change detections 9 and 10) are characterized by a
higher number of pixels (Fig. 5c).

The occurrence and location of ~~these~~ secondary failures (blue pixels in Fig. 6) were not known before our analysis because
not reported by news and local government websites, and also missing in the maps of the Copernicus Emergency
Management Service (<https://emergency.copernicus.eu/mapping/list-of-components/EMSR270>) activated for the disaster
415 response. The general lack of information related to these failures was likely due to a series of issues affecting both the field
and the satellite surveys in the aftermath of the M6.7 earthquake. In fact, an effective assessment in the field was impeded by
the road damages caused ~~also~~ by the mass movements triggered by the previous major M7.5 event, whereas the use of
optical satellite images was hampered by a widespread cloud cover that, as stated before, persisted during several weeks after
the two main seismic shaking. The first information about the occurrence of these landslides ~~were-was~~ provided online by
420 Petley (2018b), about one month later, without a clear indication of their relationships with the M6.7 earthquake. The
detection of this second set of failures in areas poorly affected by ~~previous~~ slope movements triggered by the ~~M7.5~~
~~event~~ ~~mainshock~~ demonstrates the relevant usefulness of the proposed processing chain.

~~The segments located outside the landslide affected areas are caused by other land cover changes that are out of the aims of
this study, or by random noise effects. Segments related to these changes can be easily identified because composed by an
425 average number of pixels close to ten, as detected in all the change detections, whereas segments related to landslides (i.e.
change detections 9 and 10) are characterized by a higher number pixels (Fig. 5c).~~

A suitable segmentation can allow hence to get statistical evidences of event landslides occurrence. Statistical distributions
of the three parameters shown in Fig-~~ure~~ 5 provided distinctive signatures of widespread land cover changes triggered by the
M7.5 mainshock and by the M6.7 aftershock. It is worth noting, however, that 95-percentiles highlighted in the plots are
430 exceeded also by other peaks (e.g., change detection 13 in the segment count), that cannot be considered as diagnostic of
landslide occurrence since they are ephemeral, and are not steady in all the three plots as the change detections 9 and 10. In
case of small-scale landslides occurring in localized portions of a wide area, the related statistical signals may result
imperceptible if these are of the same magnitude of other previous and successive signals not related to landslides. In cases
like this, distinctive evidence of slope failures can be achieved by starting the processing ~~ing~~ chain with a smaller subset of the
435 LR layer (i.e. monitored area).

~~Overlapping between the segments (i.e. change detections 9 and 10) to ground truth data revealed that largest SAR amplitude
changes correspond often with landslides (Fig. 6). A further evidenece was provided by the statistical distributions shown in
Fig. 9, resulted similar to those estimated by other landslide-related studies (Stark and Hovius, 2001; Malamud et al., 2004;
Rossi et al., 2012; Schlögel et al., 2015).~~

The outcomes of this study represent a concrete example on how to exploit the relevant advantages of Open Source software
with a command line interface (i.e. SNAP and GRASS GIS) to implement automatic processing chains. Moreover, ~~it is~~
440 ~~worth noting that~~ the proposed methodology can be properly adopted to monitor areas in the order of thousands of square

kilometers if powerful hardware resources are available. In fact, the pre-processing and segmentation steps require significant amounts of calculation power and memory. It is well known that the Mean Shift is a time-consuming algorithm for large datasets (Wu and Yang, 2007), and convergence for large areas can be reached in dozens of hours. Segmentation times are proportional to the dimensions of the monitored area, and to the selected spatial kernel size (*hs*).

A final remark concerns the occurrence of landslides in the study area. Generally, landslides in the mountainous sectors of Papua New Guinea are very common processes. Earthquakes with a magnitude greater than 5 are among the dominant factors triggering widespread landslides. According to Robbins and Petterson (2015), such earthquakes occur regularly in the country but records of the triggered landslides are surprisingly lacking. The lack of systematic reporting and the remoteness of communities affected by such events, also impeded an adequate characterization of landslide hazard and risk (Blong, 1986). Robbins et al. (2013) stated that landslides occur annually, and failures tend to range from few cubic meters of material to mass movements with estimated volumes of 1.8×10^9 m³, varying from debris slides, avalanches and flows to translational and rotational slides. In this framework, the landslide detection procedure described in the article may result a relevant tool for local authorities of countries characterized by extensive remote areas repeatedly affected by slope failures, and for the humanitarian organizations operating in response to geo-hydrological disasters.

5 Conclusions

This study ~~presented~~ presents a ~~semi-automatic~~ procedure aimed to support the detection of ~~rapid-moving~~ landslides inducing sharp land cover changes on vast mountainous areas. It is based on SAR data acquired systematically by the Sentinel-1 satellites. The computation of the Log-Ratio index and segmentation of the consequent raster layers allow detecting areas affected by multi-temporal variations of the radar backscattered signal. Among them, areas potentially related to rapid-moving landslides ~~are~~ can be identified with a robust statistical analysis. The performance of the implemented procedure was tested in back analysis ~~on~~ in an area of about 3000 km² in Papua New Guinea. Here, in 2018, two consecutive earthquakes (M7.5 and M6.7) triggered widespread slope failures causing more than 100 fatalities and severe damage to roads and buildings. The simulation of a multi-temporal survey of about seven months, before and after earthquakes, revealed the ability of the implemented procedure to detect statistical evidences of significant land cover changes in correspondence of the two events. Moreover, results demonstrated that the zones ~~affected~~ characterized by significant backscattering changes resulted in a reasonable agreement with those affected by landslides ~~were identified with a fair accuracy~~, as compared to the ground truth data.

The study ~~highlighted~~ highlights advantages of free SAR products that may guide the scientific community and the local authorities to develop archives of freely accessible data, suitable for implementing streamlines of information aimed to monitor natural and urbanized areas. As demonstrated in the case study, the proposed procedure has the potential to be a valid support in landslide emergency management, providing in near real-time relevant information for civil protection authorities and scientists involved in the emergency response. Future improvements may limit the user decisions in the

475 model parameterization, optimizing the processing times and refining the filtering of landslide-related changes by considering also geological and geomorphological factors.

480 **Author contributions.** GE and IM implemented the proposed procedure. AM designed the pre-processing of SAR images. GE and IM designed the segmentation procedure. GE and IM carried out the experiments. GE wrote a first draft of the manuscript. MR and GE carried out statistics about landslide-like segments. IM, GE and PR analyzed the results. GE, SS, IM and PR improved the final manuscript version. ~~IM, GE and AM designed and realized the processing chain. GE and IM carried out the experiments. GE wrote a first draft of the manuscript. MR and GE carried out statistics about landslide-like segments. IM, GE and PR analyzed the results. GE, SS, IM and PR improved the final manuscript version.~~

Competing interests. The authors declare that they have no conflict of interest.

485 **Acknowledgements.** The research was developed in the framework of the STRESS (Strategies, Tools and new data for RESilient Smart Societies) project, funded by Cariplo, focusing on designing, implementing and testing of a Spatial Information Infrastructure, enabling the provision to spatial planners and risk managers of new data and tools to improve susceptibility, hazard and impact assessment of geo-hydrological phenomena. (http://www.idpa.cnr.it/progetti_STRESS_ufficiale.html). We are grateful to Chaoying Zhao, Pierluigi Confuorto and the
490 anonymous referee for the constructive reviews and the useful suggestions.

References

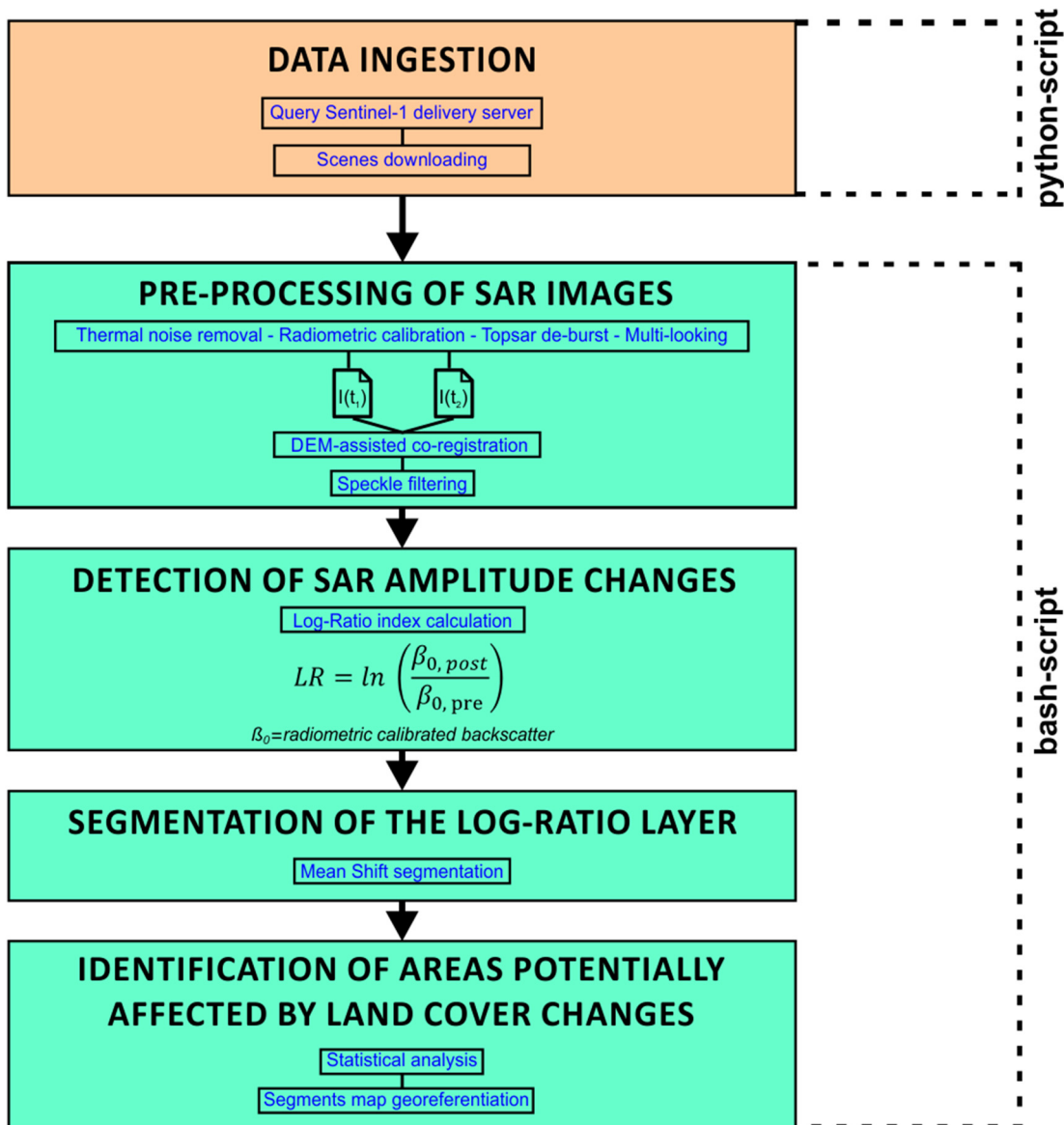
- Alvioli, M., Mondini, A. C., Fiorucci, F., Cardinali, M., and Marchesini, I.: Topography-driven satellite imagery analysis for landslide mapping, *Geomat. Nat. Haz. Risk*, 9(1), 544–567, doi:10.1080/19475705.2018.1458050, 2018.
- Blong, R.J.: Natural hazards in the Papua New Guinea highlands, *Mt. Res. Dev.*, 6, 233–246, doi: 10.2307/3673393, 1986.
- 495 Bornaetxea, T., Rossi, M., Marchesini, I., and Alvioli, M.: Effective surveyed area and its role in statistical landslide susceptibility assessments, *Nat. Hazards Earth Syst. Sci.*, 18, 2455–2469, doi:10.5194/nhess-18-2455-2018, 2018.
- Calò, F., Calcaterra, D., Iodice, A., Parise, M., and Ramondini, M.: Assessing the activity of a large landslide in southern Italy by ground-monitoring and SAR interferometric techniques, *Int. J. Remote Sens.*, 33(11), 3512–3530, doi:10.1080/01431161.2011.630331, 2012.
- 500 Calvello, M., Peduto, D. and Arena, L.: Combined use of statistical and DInSAR data analyses to define the state of activity of slow-moving landslides, *Landslides*, 14(2), 473–489, doi:10.1007/s10346-016-0722-6, 2017.
- Casagli, N., Frodella, W., Morelli, S., Tofani, V., Ciampalini, A., Intrieri, E., Raspini, F., Rossi, G., Tanteri, L. and Lu, P.: Spaceborne, UAV and ground-based remote sensing techniques for landslide mapping, monitoring and early warning, *Geoenvironmental Disasters*, 4(1), 1–23, doi:10.1186/s40677-017-0073-1, 2017.
- 505 Cigna, F., Bianchini, S., and Casagli, N.: How to assess landslide activity and intensity with persistent scatterer interferometry (PSI): the PSI-based matrix approach, *Landslides* 10(3), 267–283, doi:10.1007/s10346-012-0335-7, 2013.
- Colesanti, C. and Wasowski, J.: Investigating landslides with space-borne Synthetic Aperture Radar (SAR) interferometry, *Eng. Geol.*, 88(3–4), 173–199, doi:10.1016/j.enggeo.2006.09.013, 2006.

- Comaniciu, D. and Meer, P.: Mean shift: A robust approach toward feature space analysis, *IEEE Trans. Pattern Anal. Mach. Intell.*, 24(5), 603–619, doi:10.1109/34.1000236, 2002.
- 510 Dai, K., Li, Z., Tomás, R., Liu, G., Yu, B., Wang, X., Cheng, H., Chen, J. and Stockamp, J.: Monitoring activity at the Daguangbao mega-landslide (China) using Sentinel-1 TOPS time series interferometry, *Remote Sens. Environ.*, 186, 501–513, doi:10.1016/j.rse.2016.09.009, 2016.
- El-Darymli, K., McGuire, P., Gill, E., Power, D. and Moloney, C.: Understanding the significance of radiometric calibration for synthetic aperture radar imagery, *Can. Conf. Electr. Comput. Eng.*, (May), doi:10.1109/CCECE.2014.6901104, 2014.
- 515 ESA, Thermal Denoising of Products Generated by the S-1 IPF, 2017, available at: <https://sentinels.copernicus.eu/documents/247904/2142675/Thermal-Denoising-of-Products-Generated-by-Sentinel-1-IPF> (last access: 04 January 2020).
- ESA, Level-1 SLC Products, 2018, available at: <https://sentinel.esa.int/web/sentinel/user-guides/sentinel-1-sar/product-types-processing-levels/level-1> (last access: 04 January 2020).
- 520 Fiorucci, F., Cardinali, M., Carlà, R., Rossi, M., Mondini, A. C., Santurri, L., Ardizzone, F., and Guzzetti, F.: Seasonal landslides mapping and estimation of landslide mobilization rates using aerial and satellite images, *Geomorphology* 129 (1–2), 59–70, doi:10.1016/j.geomorph.2011.01.013, 2011.
- Frost, V. S., Stiles, J. A., Shanmugan, K. S., and Holtzman, J. C.: A Model for Radar Images and Its Application to Adaptive Digital Filtering of Multiplicative Noise. *IEEE T. Pattern Anal. Mach. Intell.*, PAMI-4, 157–166, 1982.
- 525 Gabriel, A. K., Goldstein, R. M., and Zebker, H. A.: Mapping small elevation changes over large areas: differential radar interferometry, *J. Geophys. Res.*, 94, 9183–9191, doi:10.1029/JB094iB07p09183, 1989.
- Guzzetti, F., Cardinali, M., Reichenbach, P., Carrara, A.: Comparing landslide maps: a case study in the upper Tiber River Basin, Central Italy, *Environ. Manage.*, 25 (3), 247–363, doi:10.1007/s002679910, 2000.
- 530 Guzzetti, F., Mondini, A. C., Cardinali, M., Fiorucci, F., Santangelo, M. and Chang, K. T.: Landslide inventory maps: New tools for an old problem, *Earth-Science Rev.*, 112(1–2), 42–66, doi:10.1016/j.earscirev.2012.02.001, 2012.
- International Federation of Red Cross and Red Crescent Societies (IFRC), Emergency Plan of Action Operation Final Report - Papua New Guinea: earthquake, available at: https://reliefweb.int/sites/reliefweb.int/files/resources/MDRPG008dfr_0.pdf (last access: 24 January 2020), 2018.
- 535 Intrieri, E., Raspini, F., Fumagalli, A., Lu, P., Del Conte, S., Farina, P., Allievi, J., Ferretti, A. and Casagli, N.: The Maoxian landslide as seen from space: detecting precursors of failure with Sentinel-1 data, *Landslides*, 15(1), 123–133, doi:10.1007/s10346-017-0915-7, 2018.
- Kersten, Valgur, M., Marcel, W., Jonas, Delucchi, L., unnic, Kinyanjui, L. K., Schlump, martinber, Baier, G., Keller, G., Castro, C.: *sentinelsat/sentinelsat: v0.12.2 (Version v0.12.2)*, Zenodo, doi:10.5281/zenodo.1293758, 2018
- 540 Konishi, T. and Suga, Y.: Landslide detection using COSMO-SkyMed images: A case study of a landslide event on Kii Peninsula, Japan, *Eur. J. Remote Sens.*, 51(1), 205–221, doi:10.1080/22797254.2017.1418185, 2018.

- Li, N., Wang, R., Deng, Y., Liu, Y., Li, B., Wang, C., and Balz, T.: Unsupervised polarimetric synthetic aperture radar classification of large-scale landslides caused by Wenchuan earthquake in hue-saturation-intensity color space, *J. Appl. Remote Sens.*, 8, doi:10.1117/1.JRS.8.083595, 2014.
- 545 Ma, H.R., Cheng, X., Chen, L., Zhang, H., and Xiong, H.: Automatic identification of shallow landslides based on Worldview2 remote sensing images, *J. Appl. Remote Sens.*, 10(1), 016008, doi:10.1117/1.JRS.10.016008, 2016.
- Malamud, B. D., Turcotte, D. L., Guzzetti, F., Reichenbach, P.: Landslide inventories and their statistical properties, *Earth Surf. Proc. Land.*, 29(6), 687–711, doi: 10.1002/esp.1064, 2004.
- Marchesini, I., Ardizzone, F., Alvioli, M., Rossi, M., and Guzzetti, F.: Non-susceptible landslide areas in Italy and in the
550 Mediterranean region, *Nat. Hazards Earth Syst. Sci.*, 14, 2215–2231, doi:10.5194/nhess-14-2215-2014, 2014.
- Martha, T. R., Kerle, N., ~~Van~~-van Westen, C. J., Jetten, V. and Kumar, K. V.: Segment optimization and data-driven thresholding for knowledge-based landslide detection by object-based image analysis, *IEEE Trans. Geosci. Remote Sens.*, 49(12 PART 1), 4928–4943, doi:10.1109/TGRS.2011.2151866, 2011.
- 555 [McCue, K., Gibson, G., Love, D.: The Mainshock of 25 February 2018 and Aftershocks in the Central Highlands of Papua New Guinea. Australian Earthquake Engineering Society 2018 Conference, Nov 16-18, Perth, W.A.](#)
- Mergili, M., Marchesini, I., Alvioli, M., Metz, M., Schneider-Muntau, B., Rossi, M., and Guzzetti, F.: A strategy for GIS-based 3-D slope stability modelling over large areas, *Geosci. Model Dev.*, 7, 2969–2982, doi:10.5194/gmd-7-2969-2014, 2014a.
- Mergili, M., Marchesini, I., Rossi, M., Guzzetti, F., and Fellin, W.: Spatially distributed three-dimensional slope stability
560 modelling in a raster GIS, *Geomorphology*, 206, 178–195, doi:10.1016/j.geomorph.2013.10.008, 2014b.
- Momsen, E. and Metz, M.: i.segment, available at: <https://grass.osgeo.org/grass74/manuals/i.segment.html> (last access: 07 January 2020), 2017.
- Mondini, A. C.: Measures of spatial autocorrelation changes in multitemporal SAR images for event landslides detection, *Remote Sens.*, 9(6), doi:10.3390/rs9060554, 2017.
- 565 Mondini, A. C., Chang, K. T., and Yin, H. Y.: Combining multiple change detection indices for mapping landslides triggered by typhoons, *Geomorphology*, 134, 440–451, doi:10.1016/j.geomorph.2011.07.021, 2011.
- Mondini, A. C., Santangelo, M., Rocchetti, M., Rossetto, E., Manconi, A. and Monserrat, O.: Sentinel-1 SAR amplitude imagery for rapid landslide detection, *Remote Sens.*, 11(7), 1–25, doi:10.3390/rs11070760, 2019.
- Petley, D.: An emerging crisis? Valley blocking landslides in the Papua New Guinea highlands, available at:
570 <https://blogs.agu.org/landslideblog/2018/02/28/papua-new-guinea-crisis/> (last access: 24 January 2020), 2018a.
- Petley, D.: Papua New Guinea earthquake – continued landslide impacts, available at:
<https://blogs.agu.org/landslideblog/2018/03/14/papua-new-guinea-earthquake-3/> (last access: 24 January 2020), 2018b.
- Planet Team, Planet Application Program Interface: In Space for Life on Earth, San Francisco, CA, available at: <https://api.planet.com> (last access: 24 January 2020), 2017.

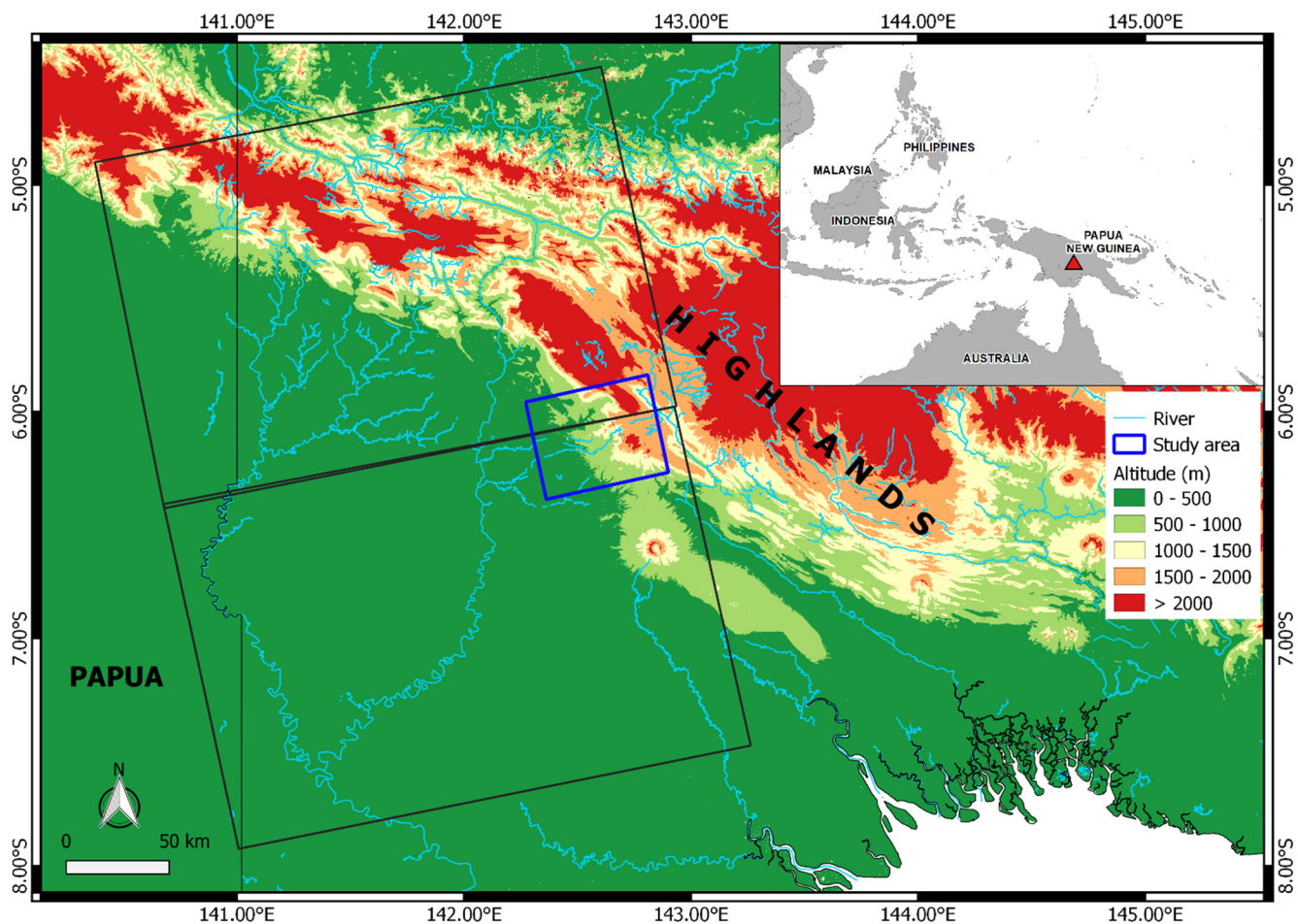
- 575 Plank, S.: Rapid damage assessment by means of multi-temporal SAR - A comprehensive review and outlook to Sentinel-1, *Remote Sens.*, 6, 4870–4906, doi:10.3390/rs6064870, 2014.
- Plank, S., Twele, A. and Martinis, S.: Landslide mapping in vegetated areas using change detection based on optical and polarimetric SAR data, *Remote Sens.*, 8(4), doi:10.3390/rs8040307, 2016.
- Raspini, F., Bardi, F., Bianchini, S., Ciampalini, A., Del Ventisette, C., Farina, P., Ferrigno, F., Solari, L. and Casagli, N.:
580 The contribution of satellite SAR-derived displacement measurements in landslide risk management practices, *Nat. Hazards*, 86(1), 327–351, doi:10.1007/s11069-016-2691-4, 2017.
- Reichenbach, P., Rossi, M., Malamud, B. D., Mihir, M. and Guzzetti, F.: A review of statistically-based landslide susceptibility models, *Earth-Science Rev.*, 180(November 2017), 60–91, doi:10.1016/j.earscirev.2018.03.001, 2018.
- Robbins, J. C. and Petterson, M. G.: Landslide inventory development in a data sparse region: spatial and temporal
585 characteristics of landslides in Papua New Guinea, *Nat. Hazards Earth Syst. Sci. Discuss.*, 3(8), 4871–4917, doi:10.5194/nhessd-3-4871-2015, 2015.
- Robbins, J. C., Petterson, M. G., Mylne, K. and Espi, J. O.: Tumbi Landslide, Papua New Guinea: Rainfall induced?, *Landslides*, 10(5), 673–684, doi:10.1007/s10346-013-0422-4, 2013.
- Rossi, M., Ardizzone, F., Cardinali, M., Fiorucci, F., Marchesini, I., Mondini, A. C., Santangelo, M., Ghosh, S., Riguer, D.
590 E. L., Lahousse, T., Chang, K. T., and Guzzetti, F.: A tool for the estimation of the distribution of landslide area in R., *Geophysical Research Abstract*, 14, EGU2012–9438–1, 2012.
- Rossi, M. and Reichenbach, P.: LAND-SE: a software for statistically based landslide susceptibility zonation, version 1.0, *Geosci. Model Dev.*, 9, 3533–3543, doi:10.5194/gmd-9-3533-2016, 2016.
- Salvi, S., Stramondo, S., Funning, G.J., Ferretti, A., Sarti, F. and Mouratidis, A.: The Sentinel-1 mission for the
595 improvement of the scientific understanding and the operational monitoring of the seismic cycle, *Remote Sens. Environ.*, 120, 164–174, doi:10.1016/j.rse.2011.09.029, 2012.
- Santangelo, M., Marchesini, I., Bucci, F., Cardinali, M., Fiorucci, F., and Guzzetti, F.: An approach to reduce mapping errors in the production of landslide inventory maps, *Nat. Hazards Earth Syst. Sci.*, 15, 2111–2126, doi:10.5194/nhess-15-2111-2015, 2015.
- 600 [Schellenberger, T., Ventura, B., Zebisch, M., Notarnicola, C.: Wet Snow Cover Mapping Algorithm Based on Multitemporal COSMO-SkyMed X-Band SAR Images. IEEE J. Sel. Top. Appl. Earth Obs. Remote Sens., 5, 1045–1053, doi: 10.1109/JSTARS.2012.2190720, 2012.](#)
- Schlögel, R., Malet, J. P., Reichenbach, P., Remaitre, A. and Doubre, C.: Analysis of a landslide multi-date inventory in a complex mountain landscape: the Ubaye valley case study, *Nat. Hazards Earth Syst. Sci.*, 15, 2369–2015, doi: 10.5194/nhess-15-2369-2015, 2015.
605
- Shimada, M., Watanabe, M., Kawano, N., Ohki, M., Motooka, T. And Wada, Y.: Detecting Mountainous Landslides by SAR Polarimetry: A Comparative Study Using Pi-SAR-L2 and X-band SARs, *Trans. Japan Soc. Aeronaut. Sp. Sci. Aerosp. Technol. Japan*, 12(ists29), Pn_9-Pn_15, doi:10.2322/tastj.12.pn_9, 2014.

- 610 Skriver, H.: Crop classification by multitemporal C- and L-band single- and dual-polarization and fully polarimetric SAR, IEEE Trans. Geosci. Remote Sens., 50(6), 2138–2149, doi:10.1109/TGRS.2011.2172994, 2012.
- Stark, C. P. and Hovius, N.: The characterization of landslide size distributions, Geophys. Res. Lett., 28, 1091–1094, doi: /10.1029/2000GL008527, 2001.
- 615 Steger, S., Brenning, A., Bell, R., Petschko, H. and Glade, T.: Exploring discrepancies between quantitative validation results and the geomorphic plausibility of statistical landslide susceptibility maps, Geomorphology, 262, 8–23, doi:10.1016/j.geomorph.2016.03.015, 2016.
- Tessari, G., Floris, M. and Pasquali, P.: Phase and amplitude analyses of SAR data for landslide detection and monitoring in non-urban areas located in the North-Eastern Italian pre-Alps, Environ. Earth Sci., 76(2), 1–11, doi:10.1007/s12665-017-6403-5, 2017.
- 620 Twele, A., Cao, W., Plank, S. and Martinis, S.: Sentinel-1-based flood mapping: a fully automated processing chain, Int. J. Remote Sens., 37(13), 2990–3004, doi:10.1080/01431161.2016.1192304, 2016.
- United States Geological Survey (USGS), Event page of the M 7.5 Papua New Guinea earthquake occurred on February 25, 2018, Available at: <https://earthquake.usgs.gov/earthquakes/eventpage/us2000d7q6/executive#executive> (last access: 07 January 2020), 2018.
- 625 van Westen, C. J., van Asch, T. W. J., Soeters, R.: Landslide hazard and risk zonation — why is it still so difficult?, B. Eng. Geol. Environ., 65, 167–184, doi:10.1007/s10064-005-0023-0, 2006.
- Wilson, A. M. and Jetz, W.: Remotely Sensed High-Resolution Global Cloud Dynamics for Predicting Ecosystem and Biodiversity Distributions, PLoS Biol., 14(3), e1002415, doi: 10.1371/journal.pbio.1002415, 2016
- Wu, K. L. and Yang, M. S.: Mean shift-based clustering, Pattern Recognit., 40(11), 3035–3052, doi:10.1016/j.patcog.2007.02.006, 2007.
- 630 Yamaguchi, Y.: Disaster Monitoring by Fully Polarimetric SAR Data Acquired With ALOS-PALSAR, P. IEEE, 100(10), 2851–2860, doi:10.1109/JPROC.2012.2195469, 2012.
- Zhao, C., Lu, Z., Zhang, Q., and De La Fuente, J.: Large-area landslide detection and monitoring with ALOS/PALSAR imagery data over Northern California and Southern Oregon, USA, Remote Sens. Environ., 124, 348–359, <https://10.1016/j.rse.2012.05.025>, 2012.
- 635 Zhao, C., Zhang, Q., Yin, Y., Lu, Z., Yang, C., Zhu, W., and Li, B.: Pre-, co-, and post- rockslide analysis with ALOS/PALSAR imagery: A case study of the Jiweishan rockslide, China. Natural Hazards and Earth System Sciences 13, 2851-2861, 2013.



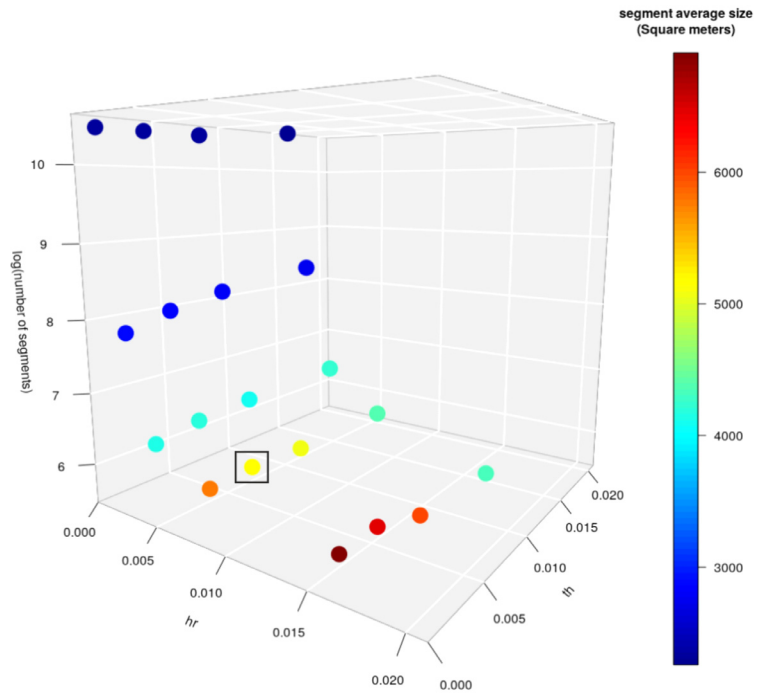
640

Figure 1: Flowchart of representing the automatic steps of the processing chain described in the text. The single steps are grouped implemented in two main-groups of scripts (developed using Python and Bash scripting languages). $I(t_1)$ and $I(t_2)$ represent two consecutive SAR images (or set of images).

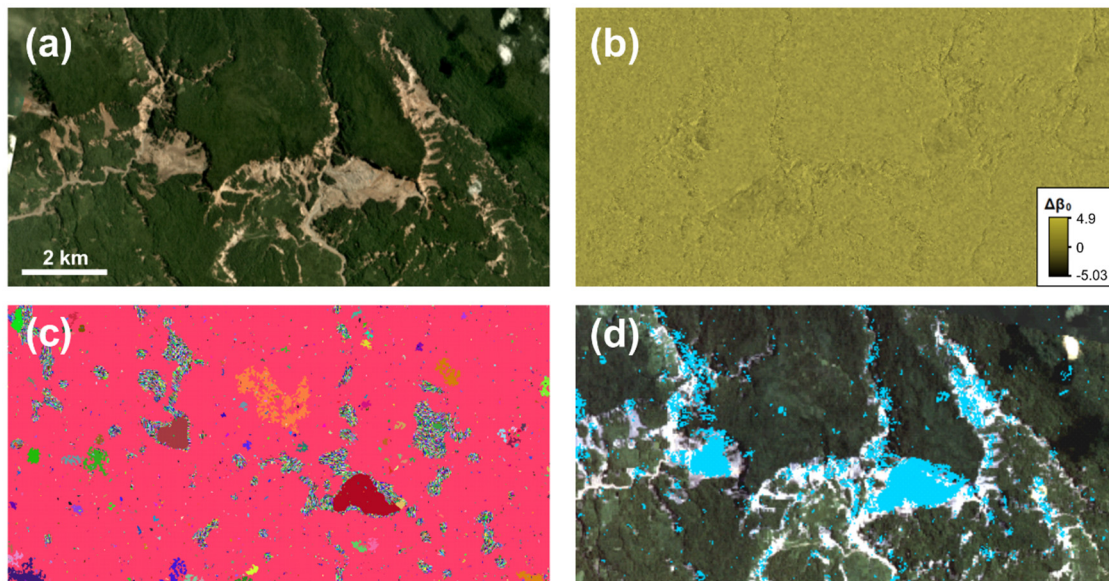


645

Figure 2: Location of the test site. The Area of Interest (AoI) is shown highlighted with a black-blue rectangle in the main map and with a red triangle in the inset. The black rectangles show the spatial coverage of the used Sentinel-1 SAR images.

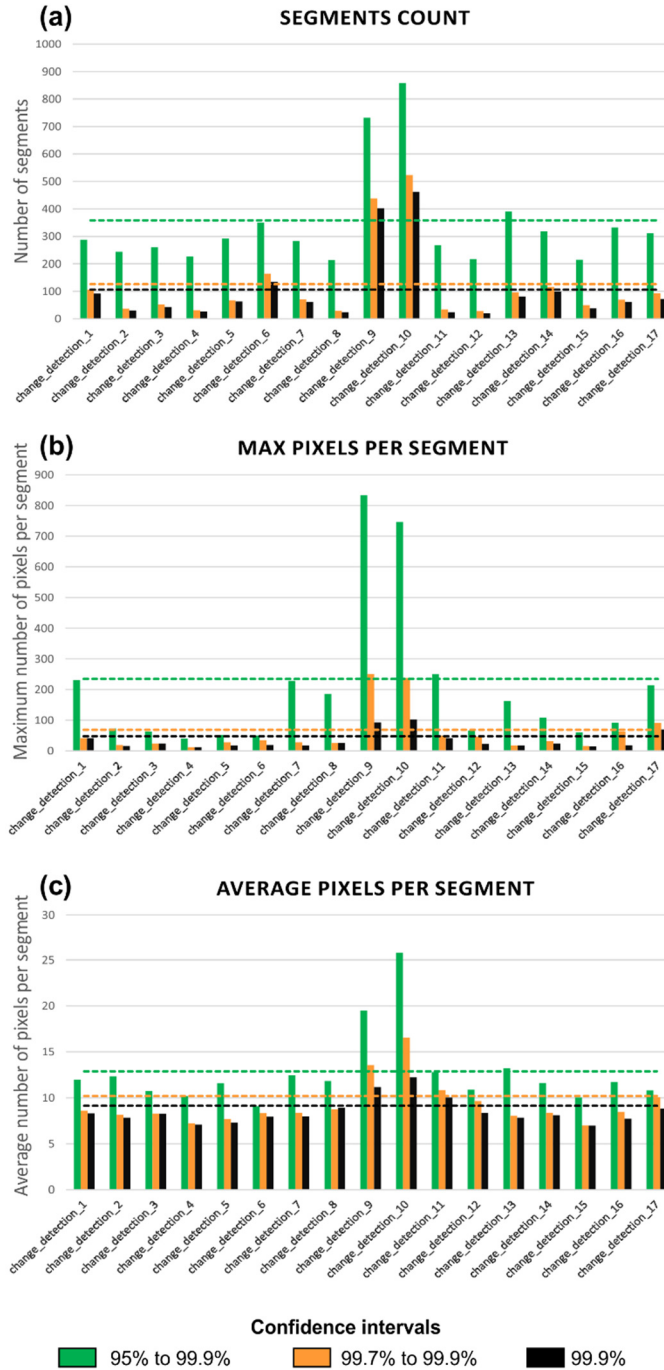


650 Figure 3 - Data analysis aimed ~~at evaluating~~to evaluate the best combination of bandwidth (*hr*) and threshold (*th*) values. The black rectangle identifies the selected combination.

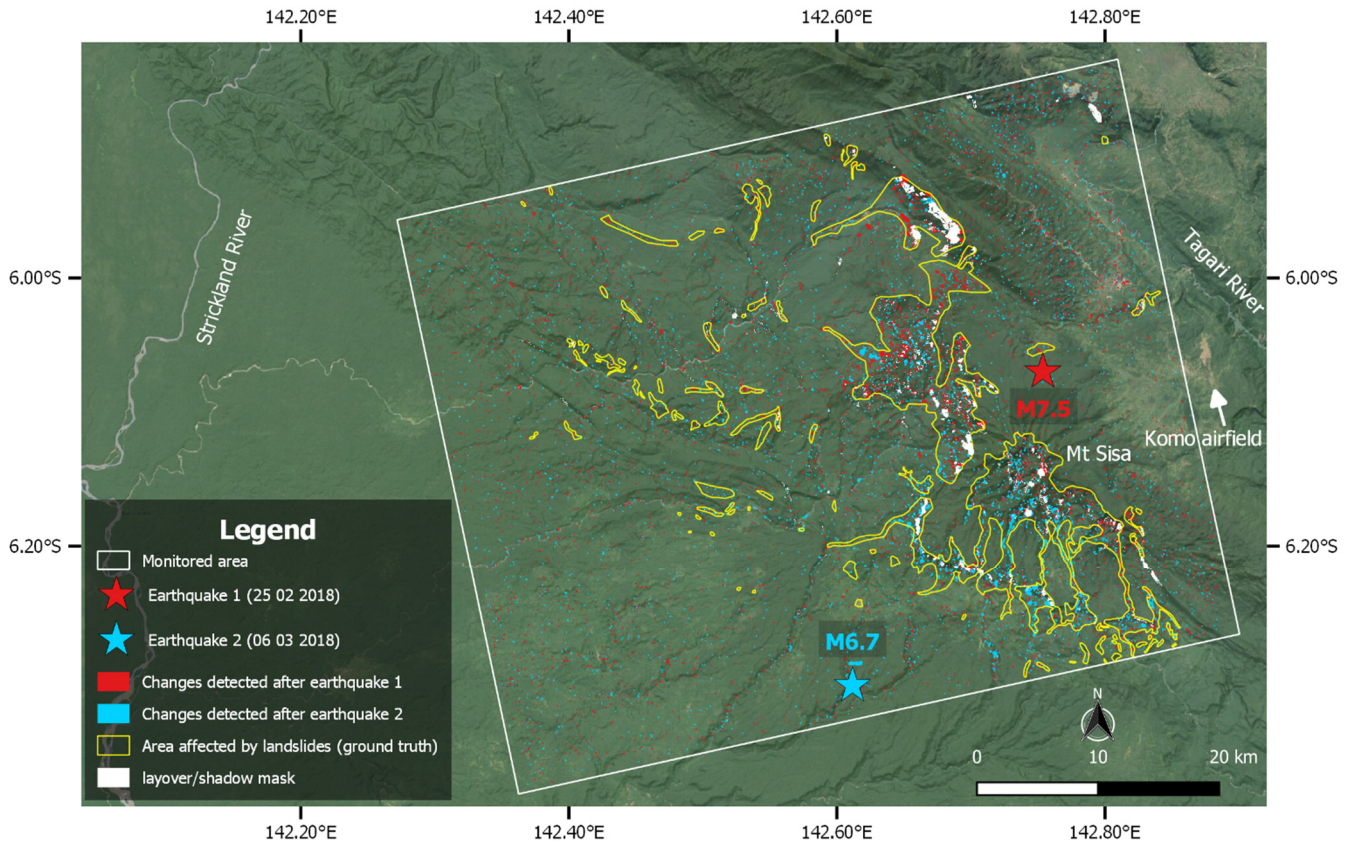


655 Figure 4 - a) Optical image of a small sample area affected by landslides within the AoI; b) the corresponding Log-Ratio layer; c) ~~the~~ the output of the segmentation algorithm (obtained using the optimized *hr* and *th* values) where the different colors are random

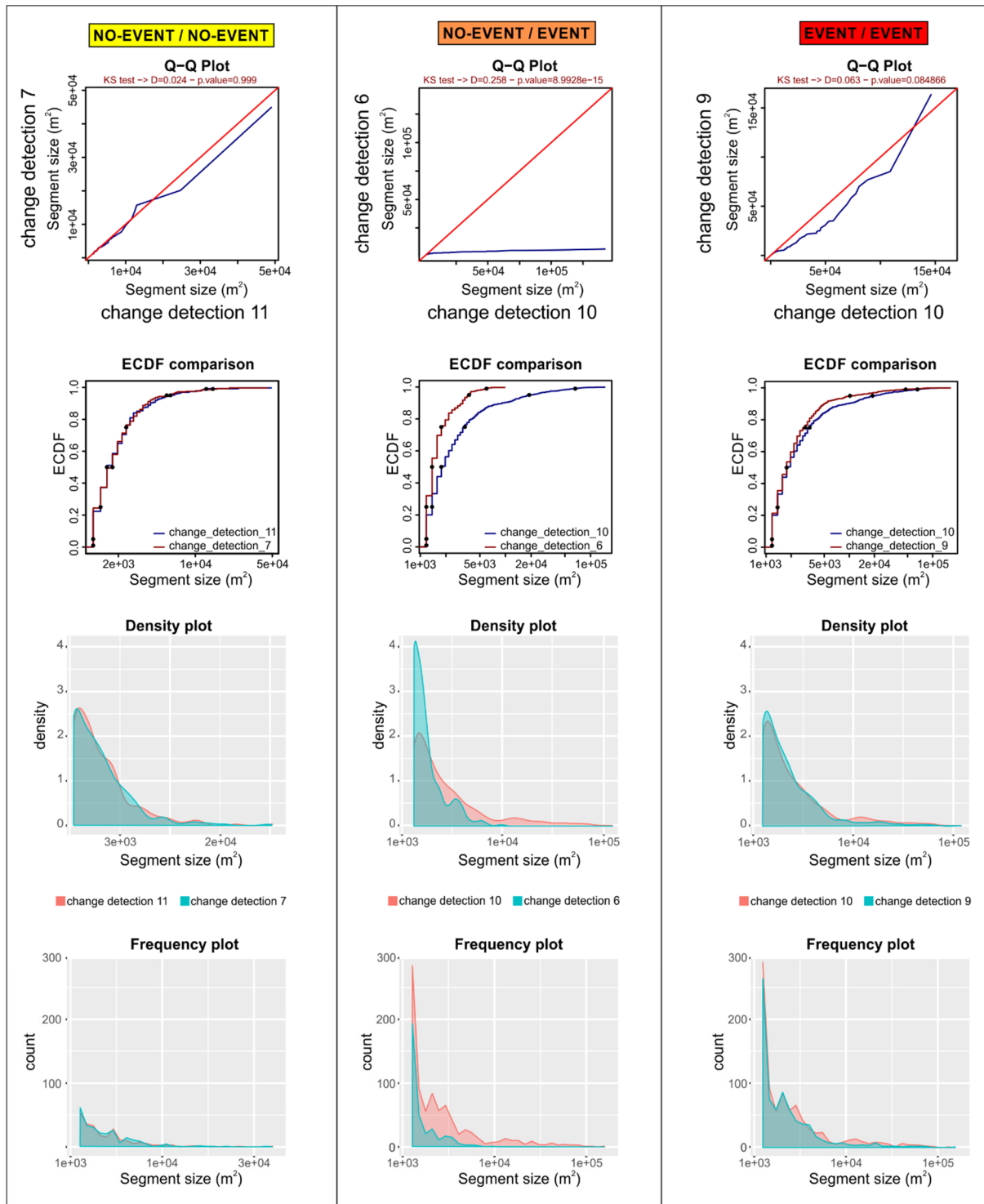
and have the only purpose to differentiate the several segments; d) the extracted landslide-related segments (in blue). Optical images have been downloaded from the Planet explorer application (Planet, 2017).



660 **Figure 5 - Statistics of the segments identified for each change detection. a) number of segments with more than 5 pixels; b-c) maximum and average number of pixels per segment. For the change detections 9 and 10, the two peaks indicate the occurrence of widespread land cover changes. The dashed lines show the 95° percentiles of the distributions (not including change detections 9 and 10).**



665 **Figure 6 - The map shows location of the epicenters of the two main earthquakes, and the distribution of segments representing SAR amplitude changes for the change detections 9 and 10. Yellow polygons are areas ~~really~~-affected by ~~clusters~~ of landslides, as ~~interpreted from optical data~~. The white rectangle identifies the AoI (see Figure 2).**



670 Figure 7 - Comparison of segment's areas statistics related to different change detections.

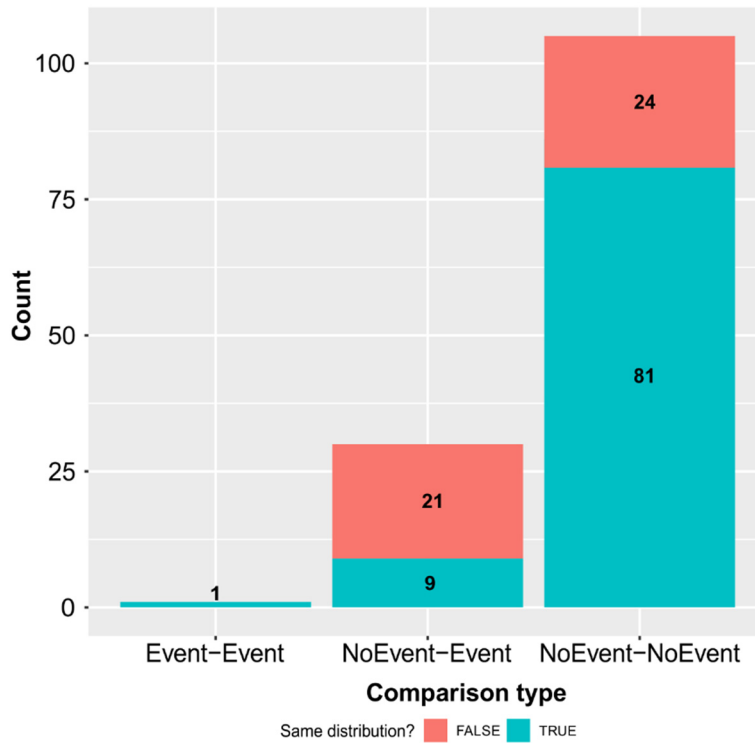
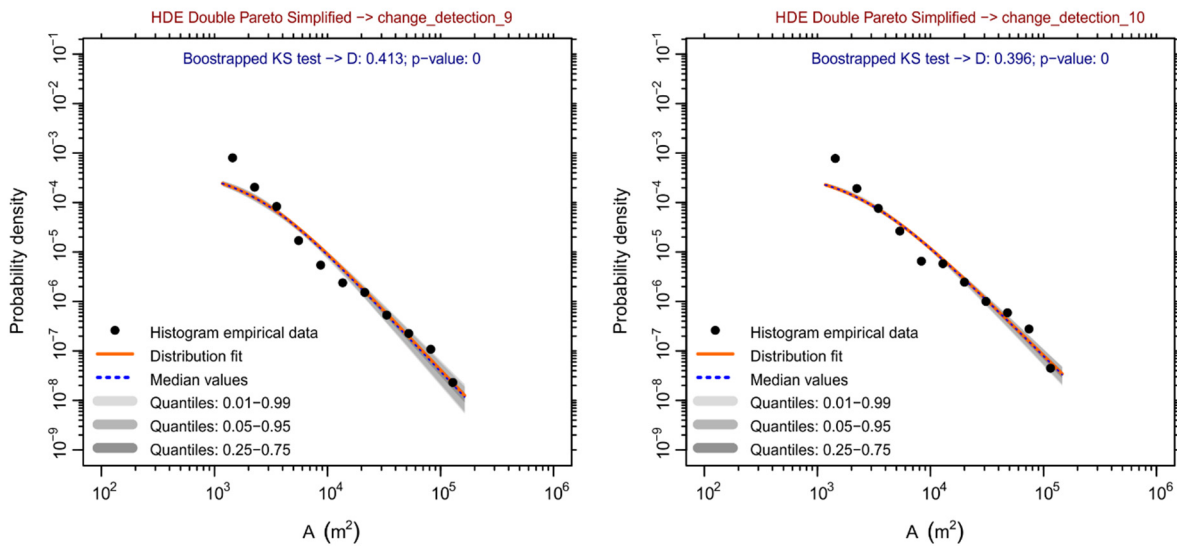


Figure 8 - Histogram representing the differences, ~~calculated according to the p-value of the Kolmogorov-Smirnov tests,~~ between all the compared ~~segment's areas distributions,~~ ~~calculated according to the p-value of the Kolmogorov-Smirnov tests.~~



675

Figure 9 - Frequency - area distribution of segments resulted in the change detections 9 (on the left) and 10 (on the right), and fitting with a Double Pareto simplified model.

Interactive comment on “A semi-automatic procedure to support the detection of rapid-moving landslides using spaceborne SAR imagery” by Giuseppe Esposito et al.

Giuseppe Esposito et al.

giuseppe.esposito@irpi.cnr.it

Received and published: 3 July 2020

General comments:

The paper entitled “A semi-automatic procedure to support the detection of rapid-moving landslides using space-borne SAR imagery” presents a semi-automatic procedure, exploiting Sentinel-1 SAR images, which evaluates changes of backscattering signals associated to land cover changes due to landsliding. The manuscript represents a solid and valuable contribution to the current state-of-the-art landslide mapping and detection during in post-emergency phases. The scientific and the applied methods are excellently depicted and supported by a robust bibliographic background. The

[Printer-friendly version](#)

[Discussion paper](#)



results are sound and consistent and supported by a very good statistical analysis, which makes the results very interesting and noteworthy. The discussion of the results in the general framework of the current literature is accurate and addresses all the concerns. The overall quality of the manuscript is very good, with an appropriate number of figures and written in an excellent English, to me. I have just a few questions which may be addressed in the discussion of the paper and which can be clarified by the authors.

Author response: We are grateful to the Reviewer for the valuable comments and suggestions relevant for the improvement of the manuscript. Point-by-point responses to all comments are outlined below. The proposed changes to the text and Figures are provided in the attached pdf file.

Specific comments

Title: The use of rapid landslide in the title can be ambiguous, since the definition of landslide magnitude can be obtained by assessing the intensity or the velocity. It is indeed a movement triggered by sudden events such as earthquakes, however, considering the current timespan between two S1 images. The same aspect should be clarified when using this expression throughout the text.

Author response: We agree with this comment. Both the title and some sentences in the text have been modified accordingly. In addition, this aspect has been explained into the Introduction section, by specifying that we focus on rapid-moving landslides since they determine more evident land cover changes with respect to slow-moving mass movements.

Dataset: I think that more information about the dataset used should be provided. A short reference within the text or by adding a table, along with the frame outline to be inserted in Figure 2, would be more appropriate.

Author response: Information on the dataset has been provided both into the sections

[Printer-friendly version](#)[Discussion paper](#)

2.1 and 3. Further specifications have been inserted in section 3, as highlighted below:

“Considering that the majority of the slopes in the study area are exposed towards West, to limit geometrical distortions in the single images and in the change detection estimation, we preferred to use IW-SLC products acquired in ascending mode, with a VV-VH polarization. Each IW product is collected with a swath characterized by a width of 250 km, subdivided in turn to three sub-swaths containing one image per polarization consisting of a series of bursts which are processed as independent SLC images.”

A new version of Figure 2, including the spatial extent of the used Sentinel-1 SAR images, has been also prepared, as shown in the attached pdf file.

Speaking of the dataset, what about the geometry of acquisition? Did you use ascending or descending images? Moreover, do you expect differences in the final results by using both geometries? I also think a short comment on the potential geometric distortions of SAR imagery should be added in the text, if in somehow this may affect the goodness of the results.

Author response: In chapter 3 we have specified that this first application of the processing chain is based only on images acquired in ascending mode. This choice was taken a priori, taking into account that most of the slopes in the study area are exposed towards West, with the aim of limiting the inclusion of geometrical distortions. Besides this, we appreciate this valuable comment that gives us a starting point for improving the proposed procedure and considering the descending images in future steps. We agree that images acquired in both geometries can improve the quality of results, especially in mountainous areas. However, in this first application we focused mainly on the implementation of the processing chain, trying to get reasonable results in terms of output to a real case study. In the next steps, we will work to improve both detection and localization of landslide-related land cover changes, taking into account the possibility of combining ascending and descending images. We have added short comments in the Discussion section, as requested by the Reviewer.

[Printer-friendly version](#)[Discussion paper](#)

Structure of the paper: I find ambiguous to write about the results when speaking of the test site. I find more appropriate to separate the result section from the paragraph 3, by adding a fourth paragraph which should address only the results obtained.

Author response: We structured the paper by describing firstly the implemented procedure, and subsequently the application in Papua New Guinea. The latter is described within the chapter 3 that is thus aimed at outlining the results obtained with the procedure described before. For this reason, we propose to do not change the structure of the paper.

Results: Do you think all the changes detected, even those within the ground truth landslides, can be attributed to landslides? Are there any other land cover changes that can be identified (e.g. deforestation, river deviation, noise, etc.)? You write, indeed (line 301), that many segments outside landslide areas are not attributable to landslides, however, it is possible to find these segments within the ground truth landslides? Do you think is sufficient to discriminate landslide and non-landslide pixels by their number?

Author response: Thanks for this comment that allows us to clarify this crucial point of the paper. It is possible to find segments related to noise and local stream changes also within the yellow polygons, where landslides occurred. However, segments related to these type of changes are relatively smaller than those ascribable to landslides, as shown in the unchanged zones represented in Figure 4(d). The occurrence of many and large landslide-related segments has strongly influenced the statistics of change detections 9 and 10 shown in Figure 5, with respect to the other change detections characterized mostly by noise-related smaller segments. Therefore, both the size and the number of segments resulted discriminant for landslides detection. We exclude changes related to earthquake damage into the yellow polygons, given that the study area is sparsely populated.

I think the classification of the detected segments is still a main challenge, which, of

[Printer-friendly version](#)[Discussion paper](#)

course, could be addressed in future work. In this sense, do you think that a validation/comparison with other techniques and other data (e.g. PolSAR, OBIA, InSAR, DTM change detections) may help to better classify land cover changes segments?

Author response: We agree with the Reviewer. A future integration of different types of data and techniques may be useful to better classify the land cover changes and improve the landslides detection. Data at higher spatial and temporal resolution providing different types of information, for example, may allow validating and/or improving the current outcomes. However, it is worth noting that one of the strengths of our procedure is the use of data that are freely accessible, and with a constant revisiting time. This supported us in implementing an automatic processing chain.

Technical comments:

Line 96: please, specify that slightly better than 5 m by 5 m spatial resolution is when dealing with StripMap acquisition mode.

Author response: We agree with this comment. The sentence has been modified as follows:

“Satellites Sentinel-1A and 1B acquire images characterized by pixels with sizes ranging from 5 (range) \times 20 (azimuth) m in the default acquisition mode for land observations (Interferometric Wide Swath mode - IW) up to 5x5 m, in the Strip Map mode”.

Figure 2: as I said in a previous comment, SAR dataset frame could be added here to have a complete overview of the study area.

Author response: We agree with this comment and a new version of Figure 2, including the spatial coverage of the used Sentinel-1 SAR images, has been prepared. Please, see the attached pdf file.

Figure 4: please, add a color bar where necessary and the source of the optical image used.

[Printer-friendly version](#)[Discussion paper](#)

Author response: We added a color bar only in the Figure 4(b), since it was missing in the early version. Further comments aimed to clarify the contents reported in the Figure 4(c), as well as the source of optical images used in the Figures 4(a) and 4(d) are added into the caption. Please, see the attached pdf file.

Please also note the supplement to this comment:

<https://www.nat-hazards-earth-syst-sci-discuss.net/nhess-2020-55/nhess-2020-55-AC1-supplement.pdf>

Interactive comment on Nat. Hazards Earth Syst. Sci. Discuss., <https://doi.org/10.5194/nhess-2020-55>, 2020.

Printer-friendly version

Discussion paper



Interactive comment on “A semi-automatic procedure to support the detection of rapid-moving landslides using spaceborne SAR imagery” by Giuseppe Esposito et al.

Giuseppe Esposito et al.

giuseppe.esposito@irpi.cnr.it

Received and published: 3 July 2020

General comments:

This research is very interested, and I think it represents a valuable contribution to the current state-of-the-art of landslide mapping and detection during post-emergency phases, especially in case of persistent clouds. The Authors apply a change-detection method, classically used in optical remote sensing, to radar images. The rational and methods are well described and presented. I agree with other comments about the title: it is somehow inexact. The main contribution of the research is the detection of earthquake-triggered landslides (event inventory mapping) rather than rapid moving

[Printer-friendly version](#)

[Discussion paper](#)



landslides detection before occurrence. Therefore, I agree to revise it. The manuscript is supported by a robust biblio-graphic background. The scientific sound is appropriate and supported by a good statistical analysis, which makes the results very interesting and noteworthy. The overall quality of the manuscript is very good, with an appropriate number of figures. The English language is good. I have just a few comments as reported in the attached pdf file.

Author response: We are grateful to the Reviewer for the appreciated comments and suggestions aimed at improving our manuscript. We agree with the previous comment. As highlighted in the attached pdf file, both the title and other issues identified by the Reviewer throughout the manuscript have been revised accordingly.

Specific comments

Please provide more information about the used images (ex. Image characteristics, geometry of acquisition).

Author response: Information on the dataset has been provided both into the sections 2.1 and 3. Further specifications have been inserted in section 3, as highlighted below:

“Considering that the majority of the slopes in the study area are exposed towards West, to limit geometrical distortions in the single images and in the change detection estimation, we preferred to use IW-SLC products acquired in ascending mode, with a VV-VH polarization. Each IW product is collected with a swath characterized by a width of 250 km, subdivided in turn to three sub-swaths containing one image per polarization consisting of a series of bursts which are processed as independent SLC images.”

A new version of Figure 2, including the spatial extent of the used Sentinel-1 SAR images, has been also prepared, as shown in the attached pdf file.

Please provide more information about georeferencing problems of radar images and associated characteristics that play a role in analysis (i.e. layover, shadow and fore-shortening).

[Printer-friendly version](#)

[Discussion paper](#)



Author response: More information about this point are provided both in the Introduction and Discussion sections, as highlighted below:

Introduction: “geometric distortions, such as layover and shadowing due to the side-looking acquisition geometry of SAR sensors, that can affect the quality of the images over mountainous areas, where landslides are likely to occur.”

Discussion: “Another improvement may consist in the use of images acquired in both ascending and descending geometries. The use of ascending images was only related to focus this first step of the work on the implementation of the entire processing chain, that we tried to simplify as much as possible. In fact, there is no doubt that combining images acquired in ascending and descending geometries can improve the quality of results, representing a non-trivial advancement of the procedure that was out of the aim of this first implementation. The a priori choice of using ascending products was based on the findings that most of the slopes in the study area are exposed towards West, with the aim of limiting the inclusion of geometrical distortions in the change detection products.”

Along the text, it is not clear which processing step is done manually, semi-automatically and in a fully automatic way. Please specify better.

Author response: Considering this comment, we probably have improperly termed the proposed procedure as “semi-automatic”. In fact, the operations described in the flowchart run in an automatic way but they need a one-time calibration phase to define both values of the parameters required for the segmentation and some statistics. Therefore, we preferred to delete “semi-automatic” from the title and within the revised version of the manuscript. Moreover, it is worth noting that information on how we automatized the described procedure is provided in the paragraph 2.5, that we have renamed as follows: “Automatic implementation of the processing chain”.

Please also note the supplement to this comment:

[Printer-friendly version](#)[Discussion paper](#)

<https://www.nat-hazards-earth-syst-sci-discuss.net/nhess-2020-55/nhess-2020-55-AC2-supplement.pdf>

Interactive comment on Nat. Hazards Earth Syst. Sci. Discuss., <https://doi.org/10.5194/nhess-2020-55>, 2020.

NHESSD

Interactive
comment

[Printer-friendly version](#)

[Discussion paper](#)



Interactive comment on “A semi-automatic procedure to support the detection of rapid-moving landslides using spaceborne SAR imagery” by Giuseppe Esposito et al.

Giuseppe Esposito et al.

giuseppe.esposito@irpi.cnr.it

Received and published: 3 July 2020

General comments:

This research is interested in by readers doing landslides inventory mapping, where SAR intensity images are employed in a large area. This method can overcome the shortage of optical images in case of cloud. The rational and procedure are introduced reasonably. However, some quantitative description of the parameters and the results need be considered carefully. Besides, the current title is somehow inaccurate. The main contribution of the research is the detection of failed landslides (event inventory mapping) rather than rapid moving landslides detection before occurrence. Therefore,

[Printer-friendly version](#)

[Discussion paper](#)



I suggest to revise the title.

Author response: We agree with this comment. The title has been modified accordingly, by deleting the term “rapid-moving” as indicated below:

“A spaceborne SAR-based procedure to support the detection of landslides”

Specific comments:

(1) Lines 95-96: “Satellites Sentinel-1A and 1B acquire images characterized by a spatial resolution up to 5x5 m, . . .”. The statement is not correct, the spatial resolutions of Sentinel-1 images are about 5 x 20 m.

Author response: This point has been clarified in the text as indicated below:

“Satellites Sentinel-1A and 1B acquire images characterized by pixels with sizes ranging from 5 (range) × 20 (azimuth) m in the default acquisition mode for land observations (Interferometric Wide Swath mode - IW), up to 5x5 m in the Strip Map mode”.

(2) Lines 135-136: “. . ., the resulting stacked images are filtered for speckling reduction using the adaptive Frost filter (Frost et al., 1982), . . .”. There are many methods to filter speckle noise in SAR images, please give some explanation to use Frost filter in this study.

Author response: We agree with the Reviewer. We chose the Frost filter following the results of some previous studies. In particular, according to Schellenberger et al. (2012), it is one of the best choices in mountainous environments, it can account for the local properties of the terrain backscatter (and landslides are local objects in this context), and it was already used successfully in previous studies dealing with landslides (Mondini, 2017). We acknowledge that using different filters we might have obtained slightly different results, and this is now discussed.

(3) Lines 146 and 128, the meaning of β_0 should be unified.

Author response: We agree with this comment. Appropriate corrections have been

[Printer-friendly version](#)

[Discussion paper](#)



done accordingly throughout the text.

(4) Due to the side-looking imaging geometry of SAR satellites, geometric distortions including layover, shadow and foreshortening are inevitable in mountainous regions, which will cause some blind areas and seriously decrease the capability of landslide detection. In this study, how did the authors deal with geometric distortions during the calculation of SAR amplitude changes?

Author response: Pixels in layover and shadows were obtained using the “SAR simulation Terrain Correction” tool available in SNAP, exploiting the SRTM 1Sec DEM, and then masked before running the statistical analysis. Foreshortening was partially mitigated by means of the reprojection procedure. We verified that the amount of the study area affected by such distortions is less than 1%.

(5) Line 583: “Flowchart of the automatic steps of the processing chain described in the text.” The authors used the terminology “semi-automatic” in title, however, in here used “automatic”. Please unify them. And the manual interaction section should be highlighted.

Author response: Considering this comment, we probably have improperly termed the proposed procedure as “semi-automatic”. In fact, the operations described in the flowchart run in an automatic way but they need a one-time calibration phase to define both values of the parameters required for the segmentation and some statistics. Therefore, we preferred to delete “semi-automatic” from the title and within the revised version of the manuscript. Moreover, it is worth noting that information on how we automatized the described procedure is provided in the paragraph 2.5, that we have renamed as follows: “Automatic implementation of the processing chain”.

(6) Figure 2: Please add the coverage of Sentinel-1 SAR images.

Author response: We accept this comment. A new version of Figure 2, including the spatial coverage of the used Sentinel-1 SAR images, has been prepared and shown in

[Printer-friendly version](#)

[Discussion paper](#)



the attached pdf file.

(7) Figure 4: (1) Please add a color bar in Figure 4(b) and (c).

Author response: We added a color bar only in the Figure 4(b), since it was missing in the early version. Further comments aimed to clarify the contents reported in the Figure 4(c), as well as the source of optical images used in the Figures 4(a) and 4(d) are added into the caption. Please, see the attached pdf file.

(8) Line 290, what do you mean the multiply 196 m² .5 (980 m²)?, Combined with the results shown in figure 6, what's the uncertainty and accuracy of the landslides detection? Moreover, what's the minimum area (size) can be detected with SAR intensity change method with high precision?

Author response: 980 m² derives from the product of a single pixel area, roughly equal to 196 m² (14x14 m² considering that 14 m is the Log-Ratio pixel size calculated after the multi-looking process), times 5 that is the minimum number of pixels included within a segment. We decided to use 5 pixels after a general evaluation of the preliminary landslide-related images published on news websites and social networks, and considering that the detection of smaller segments in the test area was not significant at the scale of our analysis. Therefore, 980 m² is a minimum area that we retained as potentially affected by a landslide. Moreover, our procedure is not aimed at landslide mapping but at a preliminary detection and rough localization of landslides, considering as minimum area affected by landslides the one selected according to the decided pixel threshold only.

(9) Figure 6: The obtained results look not good compared with the previous studies (Tessari et al., 2017; Konishi and Suga, 2018) of SAR amplitude images used for landslide detection. Such a result used directly in the detection of landslides will cause serious mis-interpretation. On the other hand, the authors should compare the landslide detection results with the ground truth to evaluate the accuracy and reliability of the method presented in this study, rather than just superimpose the SAR amplitude

changes on the ground truth. Here some quantitative assessments will be better for this method.

Author response: Thank you for this comment that gives us the opportunity to explain better a relevant point of our work. Both the cited studies were based on X-band SAR data acquired at high resolution and focused on areas smaller than the one analyzed in our study. This allowed both detection and mapping operations with a relatively high accuracy. In addition, both studies refer to geographic areas with different geological, geomorphological and land use properties with respect to the one analyzed in this work, which are also exposed to different landslide typologies. In the light of this, we believe that suitable comparisons should be possible if the same data were applied in the same area with similar techniques. Besides this, we would highlight that we present an attempt that use freely accessible C-band data, exploiting their constant availability with respect to other SAR products. The aim of the processing chain is in fact the early detection and localization of land cover changes induced by landslides over wide areas (i.e. thousands of square kilometers). The Figure 6 shows that the calculated segments concentrate mostly in the yellow polygons, where numerous landslides really occurred in the field. Considering this a first test, we retain the outcome satisfactory. Further detailed analyses, aimed at reducing some limitations of the used data, should be done for future improvements of the processing chain.

(10) Still in Figure 6, the shapes of yellow polygons do not look like landslide, especially the ones close to epicenter of M7.5. So I wonder the surface changes even in the yellow polygons are not landslides but earthquake damage. Can you verify the results?

Author response: The yellow polygons in Figure 6 (see legend) highlight the areas affected by landslides. The polygons were drawn independently from the segmentation, by means of a rough interpretation of optical data, with the aim of delimiting areas where landslides occurred in the field. In the test area, we did not perform a detailed mapping since we consider it out of the aims of the study. We used the yellow polygons to check whether the segments (red and blue pixels in Figure 6) obtained with our

[Printer-friendly version](#)[Discussion paper](#)

procedure were located in areas where the concentration of landslides was high and evident. We exclude earthquake damage into the yellow polygons, given that the study area is sparsely populated.

(11) In general, “rapid-moving landslides” represent the landslides which are deforming with large gradient without failures so far. Accurately, the landslides detected in this manuscript belong to the event-triggered landslides, i.e. landslides triggered by earthquakes. Please think more about it and make it express more precisely.

Author response: We agree with this comment. The title and the text have been modified accordingly.

Please also note the supplement to this comment:

<https://www.nat-hazards-earth-syst-sci-discuss.net/nhess-2020-55/nhess-2020-55-AC3-supplement.pdf>

Interactive comment on Nat. Hazards Earth Syst. Sci. Discuss., <https://doi.org/10.5194/nhess-2020-55>, 2020.

[Printer-friendly version](#)

[Discussion paper](#)

